crystals

MDPI

Electronic Supplementary Information

Structure, Conformation and Contact Analyses of Six Aromatic Diamide Diesters

Islam Ali Osman [1], Vickie McKee [2], Christian Jelsch [3] and John F. Gallagher [1,*]

[1] School of Chemical Sciences, Dublin City University, D09 E432 Dublin, Ireland
[2] Department of Physics, Chemistry and Pharmacy, University of Southern Denmark, Campusvej 55, 5230 Odense, Denmark
[3] CRM², CNRS UMR 7036, Faculté des Sciences et Technologies, Université de Lorraine, 54000 Nancy, France
* Correspondence: john.gallagher@dcu.ie

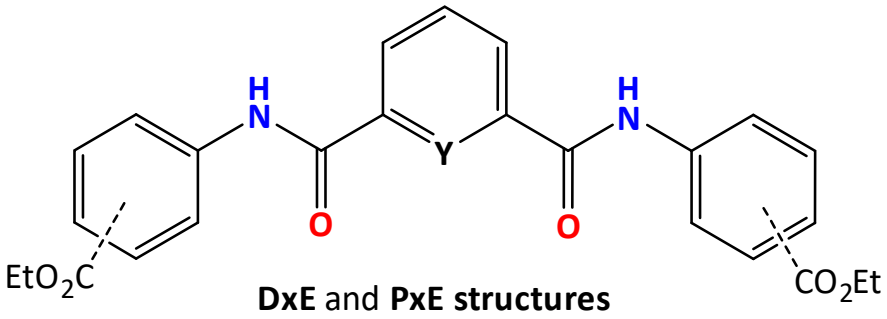

DxE and **PxE structures**

x = *ortho-*/*meta-*/*para*-ethyl ester substitution
Y = **C-H** [as **D(2/3/4)E**] or **N** [as **P(2/3/4)E**]

ESI data (in order of appearance in this supplementary electronic file):

- Chemical data for the six **DxE** and **PxE** compounds (**x** = *ortho-*/*meta-*/*para-*): pp. **S3–S18**;
- Experimental crystallographic data, tables and diagrams: pp. **S19–S22**;
- Supplementary structural diagrams (as Figures S1–S6): pp. **S23–S30**;
- Computational study of the **DxE** and **PxE** molecules: pp. **S31–S30**;
- Comparisons (overlap) of the optimised (**red**) and crystal (**blue**) structures: pp. **S37–S40**;
- Table S3: Statistical analysis of intermolecular contacts on the Hirshfeld surface: p. **S41**;
- Fingerprint plots (FPs) for **D2E–P4E**: pp. **S42–S49**;

As submitted on 24 June 2023 by
Professor John F. Gallagher,
School of Chemical Sciences, Dublin City University.

S1. Contents (Spectral Details for DxE and PxE on pp. S3–S15)

Reaction Scheme	Page S3
1. 2-EST-DIP (**D2E**)	4
1.1. ^{1}H NMR ($CDCl_3$)	4
1.2. ^{13}C NMR ($CDCl_3$)	4
1.3. ATR-IR	5
2. 3-EST-DIP (**D3E**)	6
2.1. ^{1}H NMR ($CDCl_3$)	6
2.2. ^{13}C NMR ($CDCl_3$)	6
2.3. ATR-IR	7
3. 4-EST-DIP (**D4E**)	8
3.1. ^{1}H NMR ($CDCl_3$)	8
3.2. ^{13}C NMR ($CDCl_3$)	8
3.3. ATR-IR	9
4. 2-EST-PYR (**P2E**)	10
4.1. ^{1}H NMR ($CDCl_3$)	10
4.2. ^{13}C NMR ($CDCl_3$)	10
4.3. ATR-IR	11
5. 3-EST-PYR (**P3E**)	12
5.1. ^{1}H NMR ($CDCl_3$)	12
5.2. ^{13}C NMR ($CDCl_3$)	12
5.3. ATR-IR	13
6. 4-EST-PYR (**P4E**)	14
6.1. ^{1}H NMR ($CDCl_3$)	14
6.2. ^{13}C NMR ($CDCl_3$)	14
6.3. ATR-IR	15

Chemical data for all six **DxE** and **PxE** compounds (reaction scheme for **DxE** and **PxE**);
Reaction procedure (yields) for the **DxE** and **PxE** syntheses;
IR/NMR comparison plots/melting-point details and summary for **DxE** and **PxE**;
Comparison of the aromatic regions and N-H position in $CDCl_3$;
Crystal structure details: tables of experimental and hydrogen-bonding interactions;
Supplementary structural diagrams for six **DxE**/**PxE** structures;
Computational study of the **DxE** and **PxE** molecules;
Comparisons (molecular overlap) of the optimised (**red**) and crystal (**blue**) structures;
Statistical analysis and fingerprint plots.

S2. Reaction Scheme for DxE and PxE

The reactions of ethyl-2-aminobenzoate, ethyl-3-aminobenzoate and ethyl-4-aminobenzoate with isophthaloyl dichloride for **DxE** or 2,6-pyridinedicarbonyl dichloride for **PxE** in the presence of an organic base (triethylamine) (**Scheme S1**) yielded six products as high-melting, white–yellowish-white solids. All six compounds were characterised using ^{1}H and ^{13}C NMR spectroscopy, infrared spectroscopy and single-crystal X-ray diffraction.

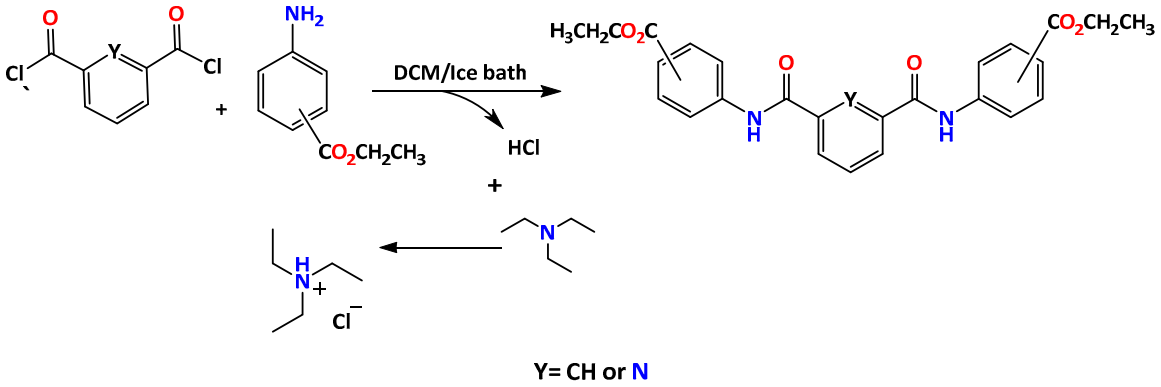

Scheme S1. Synthetic reaction scheme.

S3. Reaction Procedure for the DxE Syntheses

Isophthaloyl dichloride (2.03 g, 10 mmol) was suspended in 40 mL of dichloromethane (DCM). The flask was cooled in a water/ice bath, and either ethyl-**x**-aminobenzoate (**x** = 2, 3 or 4) (20 mmol) was added. After 10 min of stirring, triethylamine (3.49 mL, 25 mmol) was added. The reaction mixture was stirred overnight at room temperature to give a pale-yellow solution; this was poured into a separating funnel and washed with 10% aqueous ammonium chloride (NH_4Cl) solution, repeated two times, and it was then washed with distilled water five times. The solution was dried using $MgSO_4$, and coloured impurities were removed with the addition of 50 mg of active charcoal. The solvent was removed using a rotary evaporator and a white powder was collected for each of the three reactions as **DxE** (**x** = 2-, 3-, 4-). For spectral labels, **x-Est-DIP** (original) is often used instead of **DxE**. All six **DxE** and **PxE** reactions gave reasonably high yields of pure products. The reactions yields were 55–65% for both **D4E** and **P4E**. For the other isomers, the yields were higher: from 80% to 90%. Although this purification was enough for most reactions, recrystallisation in different solvents was performed for some products to eliminate impurities.

Chemicals: The ethyl 2-/3-/4-aminobenzoates, isophthaloyl dichloride, 2,6-pyridinedicarbonyl dichloride, Et_3N, NaOH, Na_2CO_3, and *conc*. HCl, $KHCO_3$, $MgSO_4$, reaction/crystallisation solvents and silica (Davisil) were used as purchased (Sigma Aldrich); TLC alumina and silica plates were from Fluka. Melting points were measured on a Stuart Scientific SMP40 automated melting-point apparatus. IR spectroscopy used a Perkin Elmer Spectrum GX FTIR spectrometer (ATR method) (bands quoted in cm^{-1}). NMR spectroscopy used a Bruker BioSpin UltraShield NMR spectrometer (293 ± 1 K), at 400 or 600 MHz for ^{1}H and at 100.62 MHz for the ^{13}C resonance. The ^{1}H and ^{13}C spectra were recorded in $CDCl_3$; NMR chemical-shift values (δ) are in ppm, referenced to TMS and coupling constants (*J*) quoted in Hz. The ^{1}H-, ^{13}C- and IR data for the six **DxE** and **PxE** are reported below.

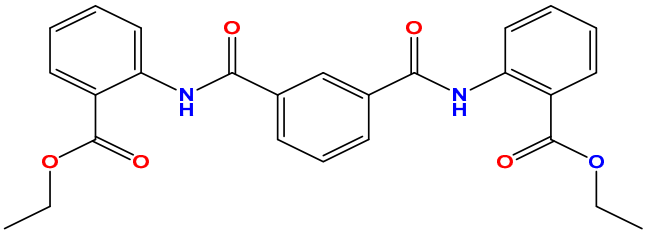

diethyl 2,2'-(isophthaloylbis(azanediyl))dibenzoate

1. **D2E** or (2-Est-DIP or) (m.p. = 204.0–206.0 °C).

1.1. ^{1}H NMR ($CDCl_3$) δ 1.36 (6H, t, ^{3}J = 7.2 Hz); δ 4.37 (4H, q, ^{3}J = 7.2 Hz); δ 7.08 (2H, td ^{3}J = 7.6 Hz, ^{4}J = 1.2 Hz); δ 7.56 (2H, td, ^{3}J = 7.9 Hz, ^{4}J = 1.7 Hz); δ 7.63 (1H, t, ^{3}J = 7.9 Hz); δ 8.06 (2H, dd, ^{3}J = 7.9 Hz, ^{4}J = 1.8 Hz); δ 8.15 (2H, dd, ^{3}J = 7.9 Hz ^{4}J = 1.9 Hz); δ 8.69 (1H, t, ^{3}J = 1.9 Hz); δ 8.87 (2H, d, ^{3}J = 8.5 Hz); δ 12.15 (2H, br s).

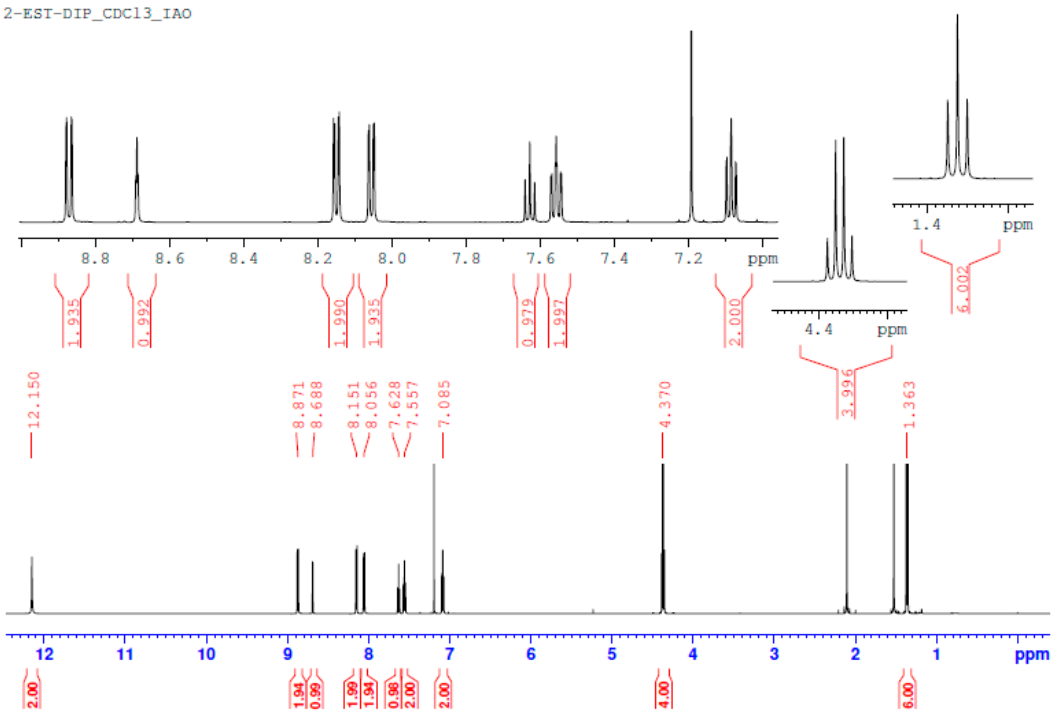

1.2. ^{13}C NMR ($CDCl_3$) δ 14.22; 30.93; 61.63; 115.67; 120.59; 122.82; 126.99; 129.38; 130.37; 130.98; 134.71; 135.84; 141.68; 164.90; 168.57.

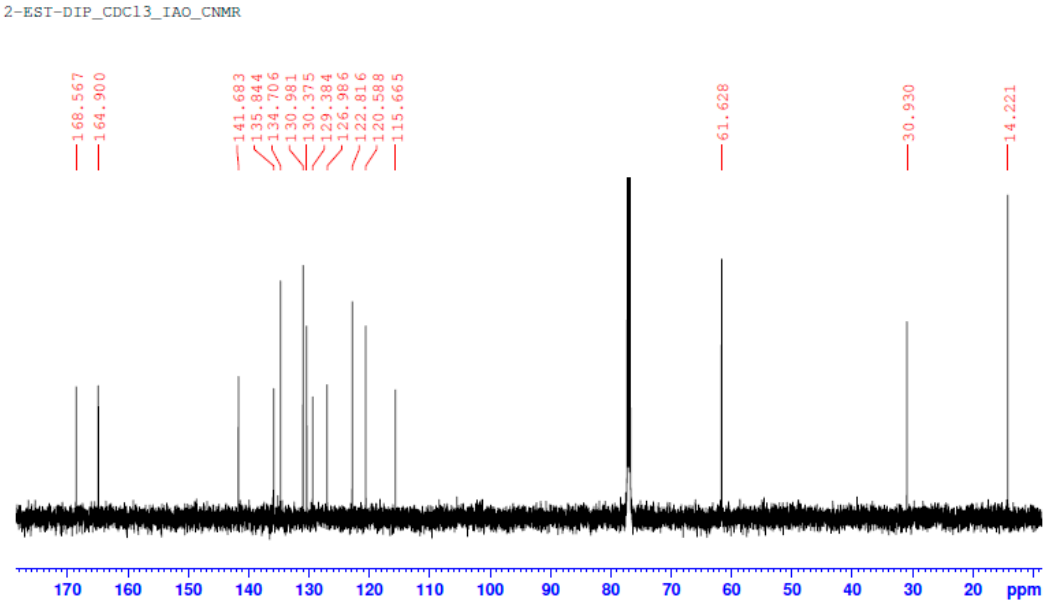

1.3. ATR-IR: 3254 (w); 2998 (w); 1678 (s); 1677 (s); 1608 (s); 1589 (s); 1540 (s); 1492 (m); 1470 (m); 1452 (m); 1365 (m); 1302 (m); 1256 (s); 1170 (m); 1070 (s); 1025 (m).

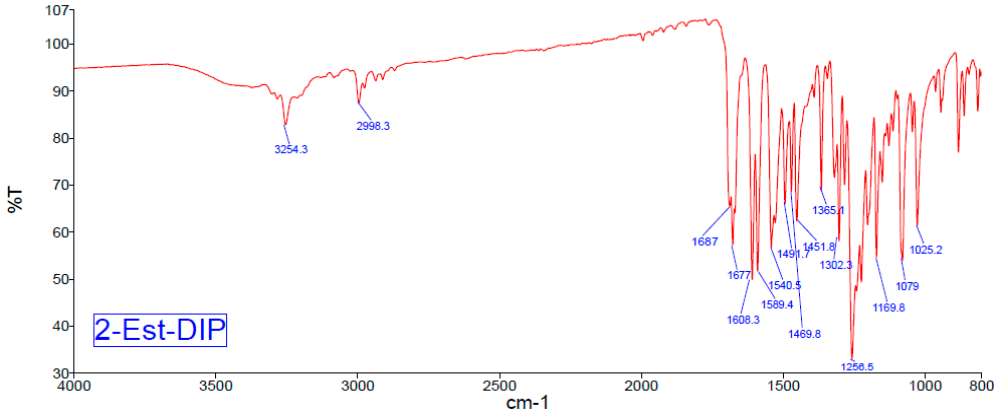

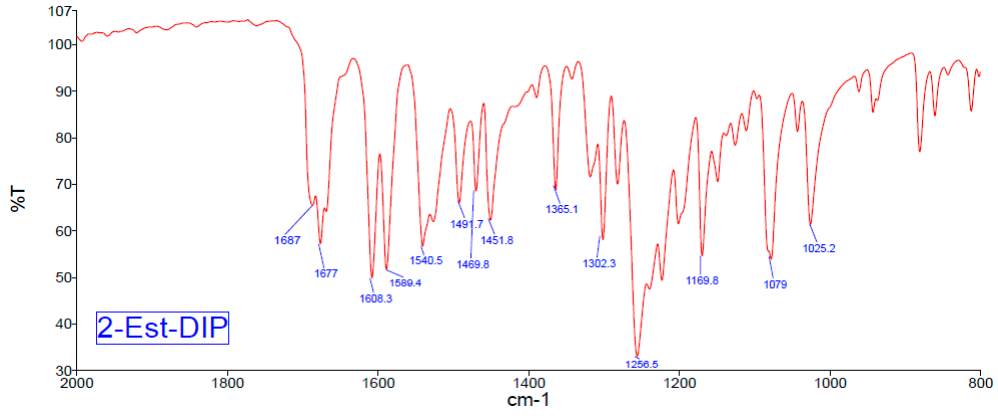

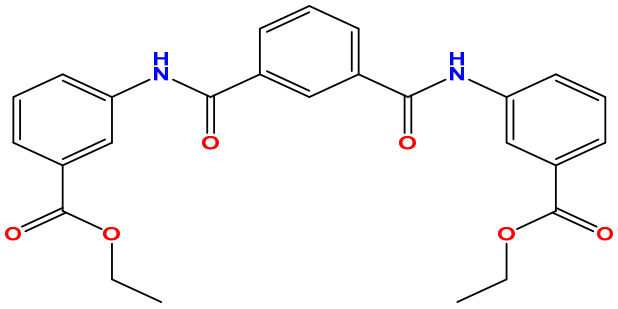

diethyl 3,3'-(isophthaloylbis(azanediyl))dibenzoate

2. **D3E** or (3-Est-DIP) (m.p. = 172.0–174.0° C).

2.1 ^{1}H NMR ($CDCl_3$) δ 1.29 (6H, t, ^{3}J = 7.2 Hz); δ 4.26 (4H, q, ^{3}J = 7.2 Hz); δ 7.34 (2H, t, ^{3}J = 8.0 Hz); δ 7.46 (1H, t, ^{3}J = 7.8 Hz); δ 7.73 (2H, dt, ^{3}J = 7.8 Hz, ^{4}J = 1.2 Hz); δ 7.95 (4H, dt, ^{3}J = 7.8 Hz, ^{4}J = 1.7 Hz); δ 8.09 (2H, t, ^{3}J = 2.0 Hz); δ 8.30 (1H, t, ^{3}J = 1.7 Hz); δ 8.47 (2H, br s).

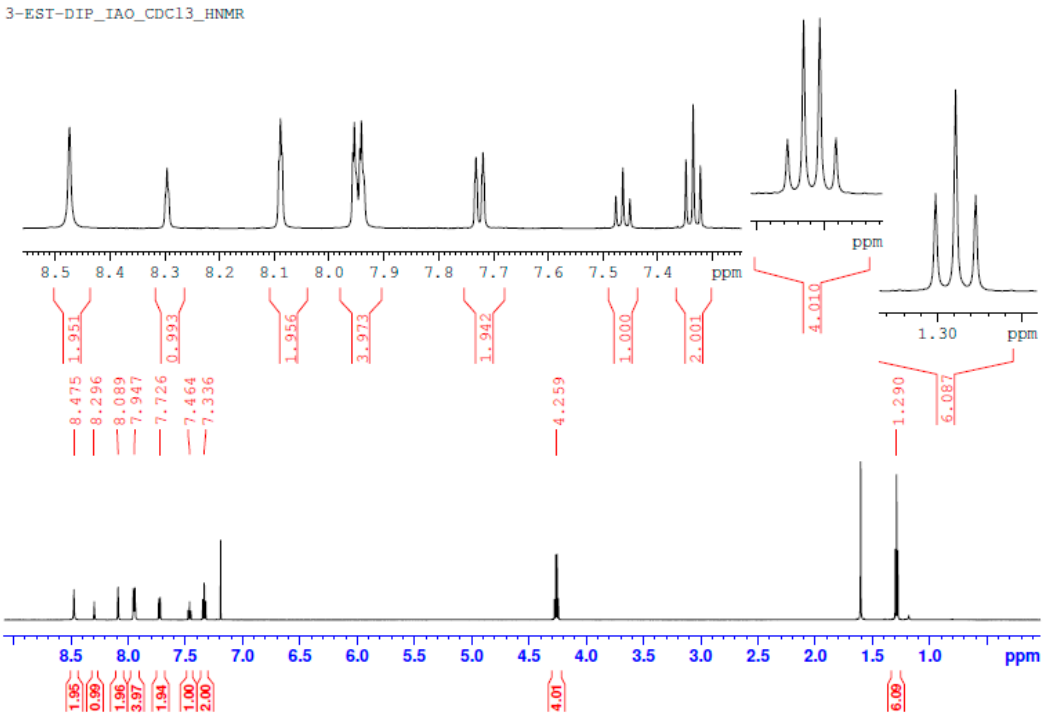

2.2 ^{13}C NMR ($CDCl_3$) δ 14.28; 61.28; 121.25; 124.78; 125.56; 125.83; 129.46; 130.72; 131.28; 135.07; 137.90; 165.09; 166.22.

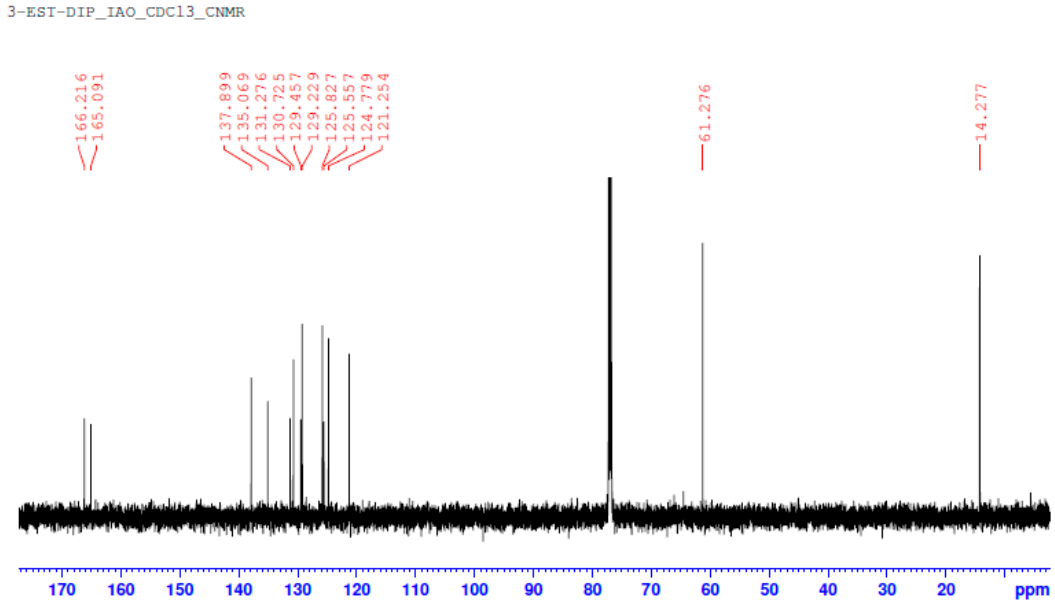

2.3 ATR-IR: 3332 (m); 2984 (w); 1717 (s); 1689 (s); 1649 (s); 1608 (m); 1537 (s); 1487 (s); 1413 (w); 1365 (m); 1305 (m); 1290 (s); 1248 (s); 1220 (s); 1172 (m); 1132 (m); 1107 (s); 1078 (s); 1025 (m).

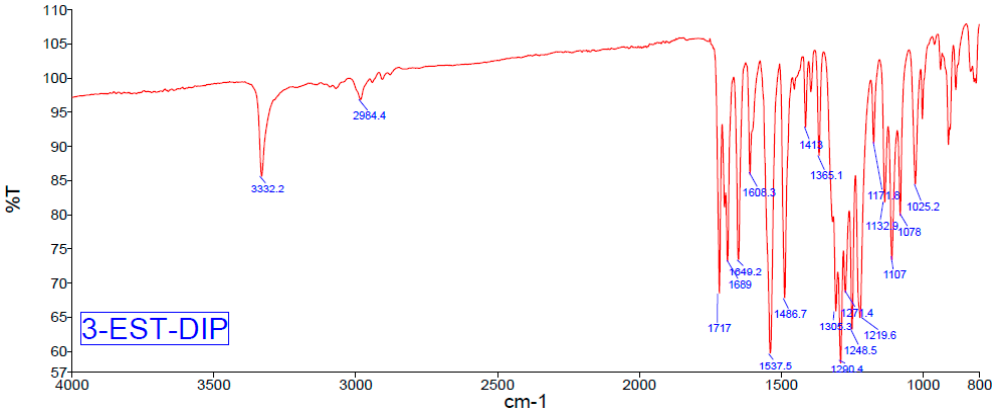

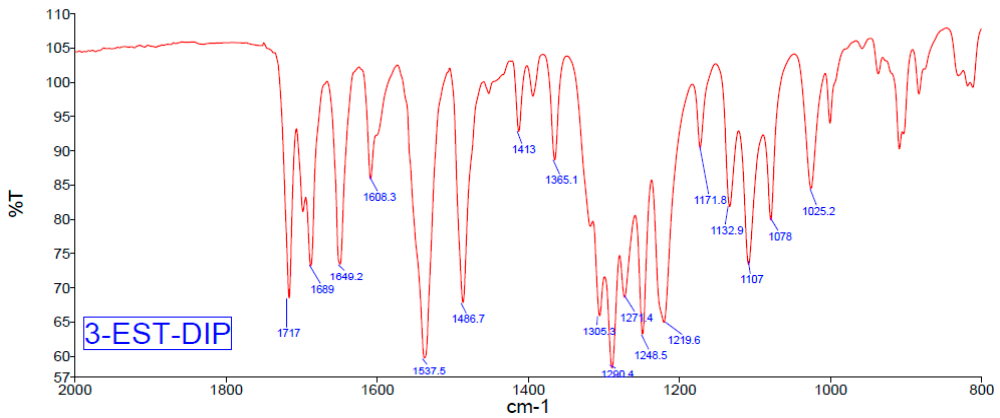

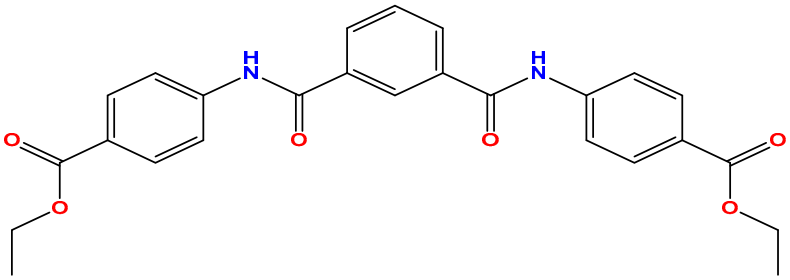

diethyl 4,4'-(isophthaloylbis(azanediyl))dibenzoate

3. **D4E** or (4-Est-DIP) (m.p. = 238.0–240.0 °C).
   3.1. ^{1}H NMR ($CDCl_3$) δ 1.34 (6H, t, ^{3}J = 7.2 Hz); δ 4.31 (4H, q, ^{3}J = 7.2 Hz); δ 7.57 (1H, t, ^{3}J = 7.8 Hz); δ 7.70 (4H, dt, ^{3}J = 8.6 Hz, ^{4}J = 2.0 Hz); δ 8.0 (6H, dt, ^{3}J = 8.6 Hz, ^{4}J = 2.0 Hz); δ 8.19 (2H, br s); δ 8.32 (1H, t, ^{3}J = 1.8 Hz).

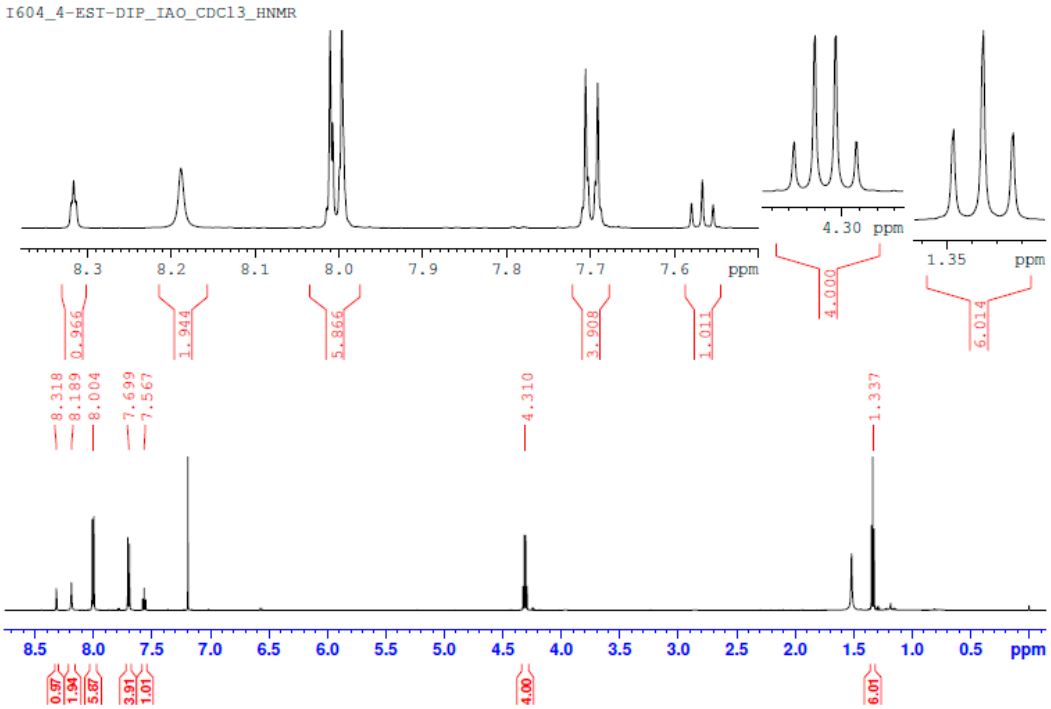

   3.2. ^{13}C NMR ($CDCl_3$) δ 14.35; 61.00; 119.35; 125.69; 126.67; 129.65; 130.68; 130.91; 135.22; 141.64; 164.72; 166.04.

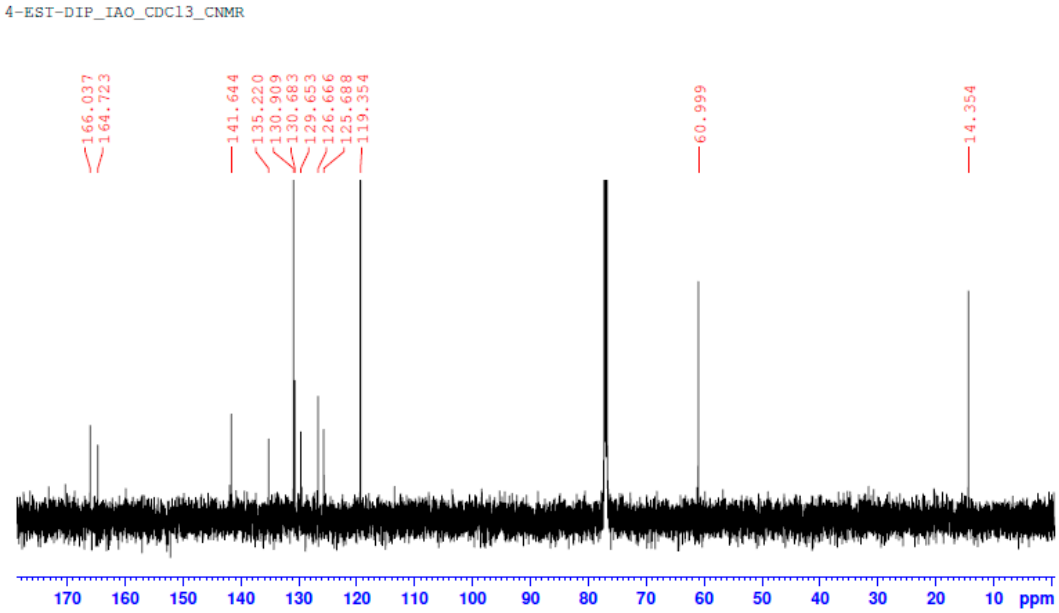

3.3. ATR-IR: 3285 (m); 2984 (w); 1712 (s); 1651 (s); 1604 (m); 1520 (s); 1408 (m); 1307 (m); 1275(s); 1173 (m); 1109 (s); 1022 (m).

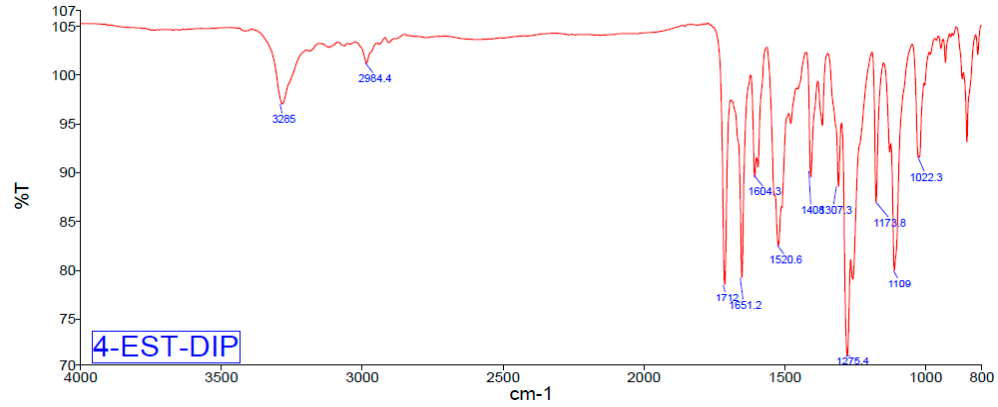

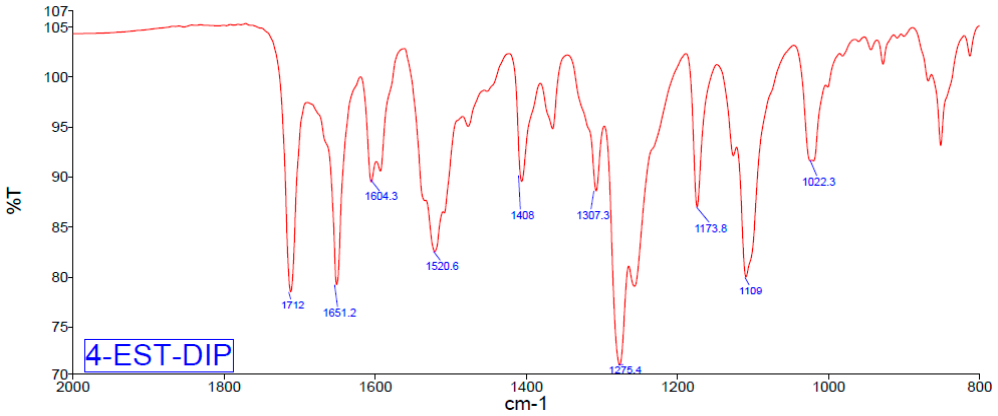

4. Reaction Group 2: The General PxE Synthetic Procedure

2,6-pyridinedicarbonyl dichloride (2.04 g, 10 mmol) was suspended in 40 mL of DCM. The flask was cooled in a water/ice bath, and either ethyl-2-aminobenzoate, ethyl-3-aminobenzoate or ethyl-4-aminobenzoate (20 mmol) was added, depending on the reaction. After 10 min of stirring, Et_3N (3.49 mL, 25 mmol) was added. The reaction mixture was stirred overnight at room temperature to give a pale-yellow solution. The reaction

mixture was then poured into a separating funnel and washed with 10% aqueous NH_4Cl solution, repeated twice, and it was then washed with distilled water five times. The solution was dried using $MgSO_4$, and coloured impurities were removed with the addition of 50 mg of active charcoal. Then, the solvent was evaporated with a rotary evaporator and the white powder of (**PxE**) (where **x** = 2-, 3-, 4-) was collected.

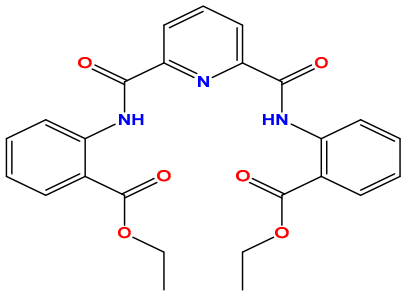

diethyl 2,2'-((pyridine-2,6-dicarbonyl)bis(azanediyl))dibenzoate

4. **P2E** or (2-Est-PYR) (m.p. = 177.0–179.0 °C).

4.1. ^{1}H NMR ($CDCl_3$) δ 1.13 (6H, t, ^3J = 7.2 Hz); δ 4.03 (4H, q, ^3J = 7.2 Hz); δ 7.12 (2H, td, ^3J = 7.6 Hz, ^4J = 1.2 Hz); δ 7.57 (2H, td, ^3J = 7.8 Hz, ^4J = 1.5 Hz); δ 8.03 (2H, dd, ^3J = 8.0 Hz, ^4J = 1.6 Hz); δ 8.07 (1H, t, ^3J = 7.7 Hz); δ 8.39 (2H, d, ^3J = 7.6 Hz); δ 8.70 (2H, dd, ^3J = 8.3 Hz, ^4J = 1.0 Hz); δ 12.68 (2H, br s).

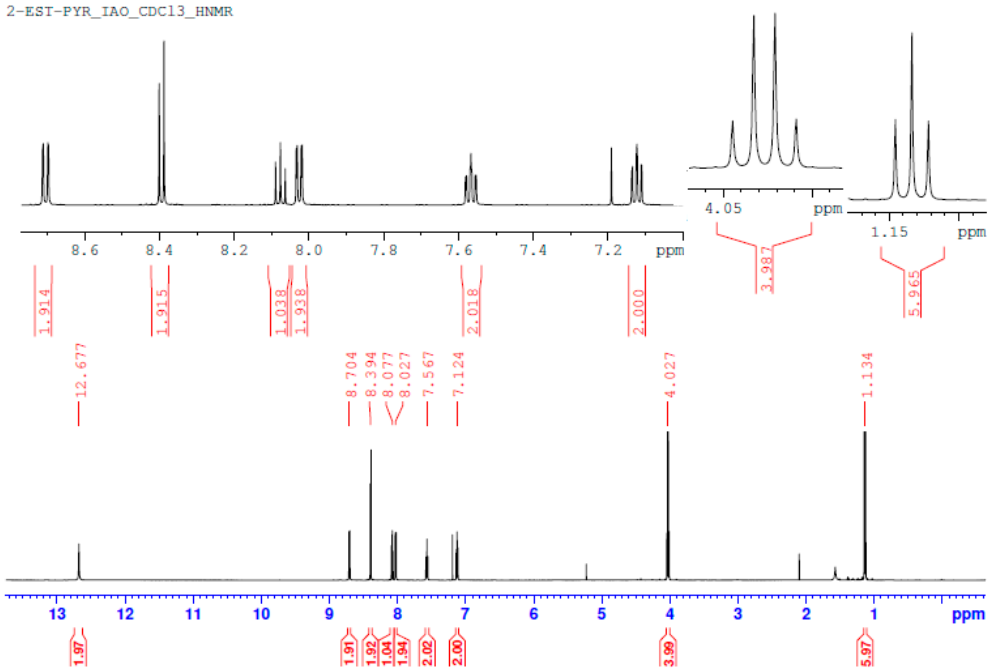

4.2. ^{13}C NMR ($CDCl_3$) δ 13.99; 61.16; 118.0; 121.62; 123.47; 125.24; 131.08; 134.14; 139.47; 140.17; 149.37; 162.19; 167.20.

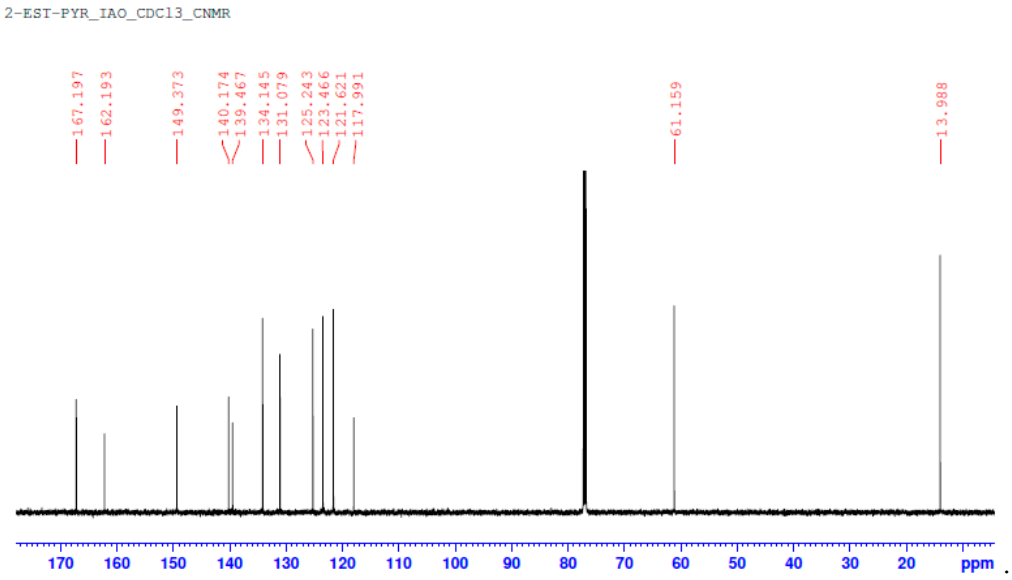

4.3. ATR-IR: 3641 (w); 3471 (w); 3338 (m); 3187 (w); 1727 (m); 1687 (s); 1675 (s); 1605 (m); 1582 (s); 1516 (s); 1490 (s); 1448 (m); 1367 (m); 1285 (m); 1254 (s); 1161 (w); 1126 (m); 1083 (m); 1000 (m).

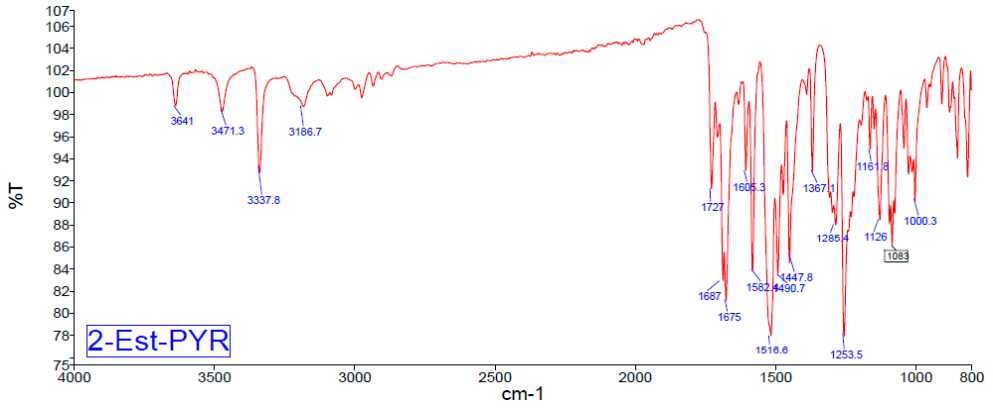

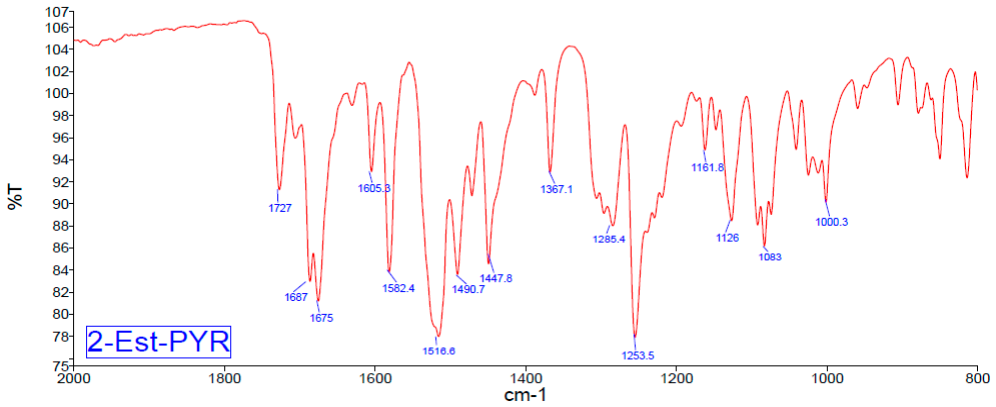

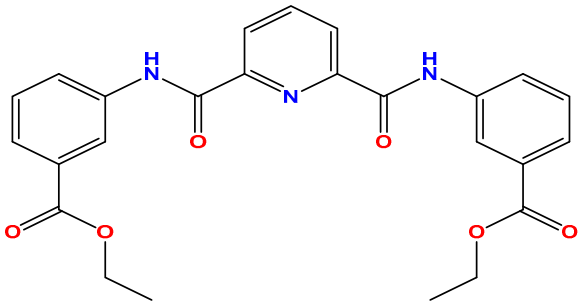

diethyl 3,3'-((pyridine-2,6-dicarbonyl)bis(azanediyl))dibenzoate

5. **P3E** or (3-Est-PYR) (m.p. = 172.0–174.0 °C).

5.1. ^{1}H NMR ($CDCl_3$) δ 1.08 (6H, t, ^{3}J = 7.2 Hz); δ 4.03 (4H, q, ^{3}J = 7.2 Hz); δ 7.33 (2H, t, ^{3}J = 8.0 Hz); δ 7.65 (2H, dt, ^{3}J = 7.9 Hz, ^{4}J = 1.2 Hz); δ 8.12 (1H, t, ^{3}J = 8.0 Hz); δ 8.38 (2H, dd, ^{3}J = 8.0 Hz, ^{4}J = 2.4 Hz); δ 8.46 (4H, m); δ 10.43 (2H, br s).

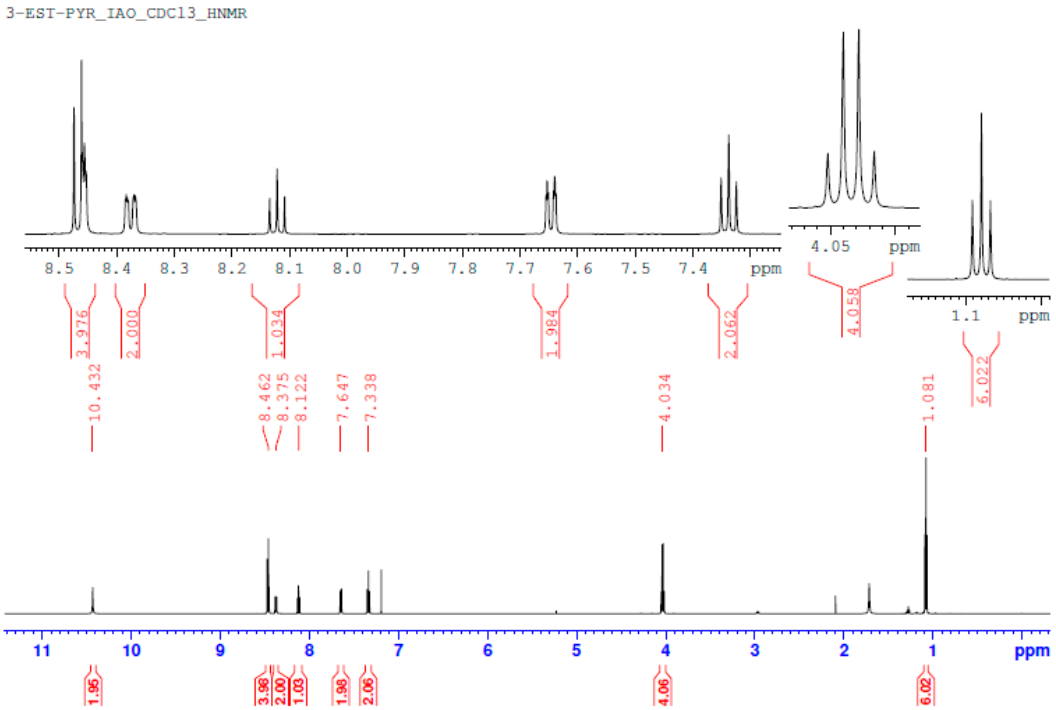

5.2. ^{13}C NMR ($CDCl_3$) δ 14.22; 60.93; 122.01; 124.28; 125.46; 125.56; 129.09; 131.02; 137.75; 139.68; 148.88; 161.34; 166.29.

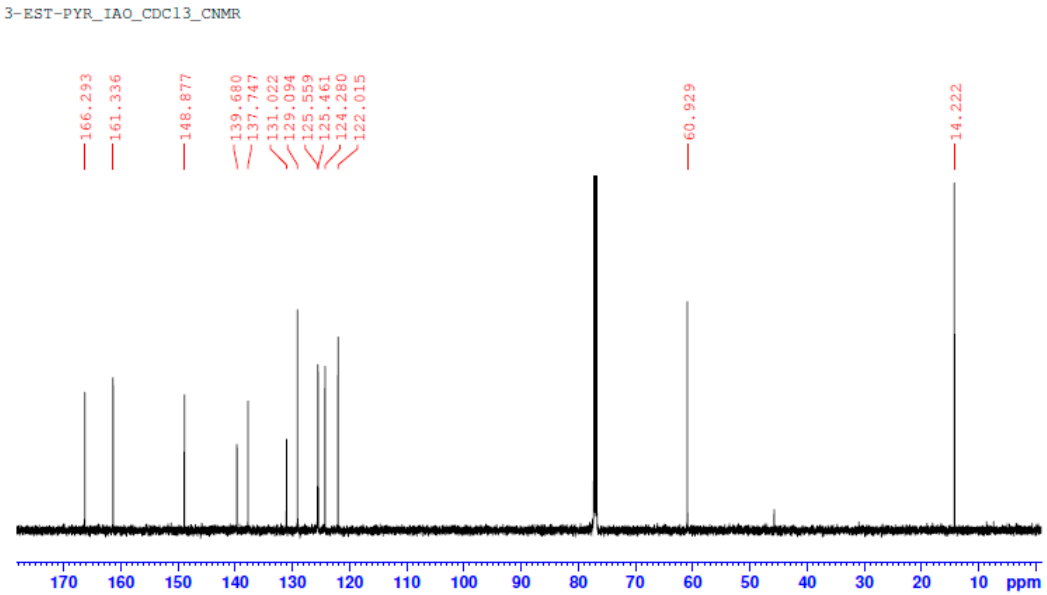

5.3. ATR-IR: 3288 (m); 2982 (m); 1718 (s); 1667 (s); 1610 (w); 1546 (s); 1487 (s); 1390 (w); 1364 (w); 1299 (m); 1276 (s); 1224 (s); 1165 (w); 1132 (m); 1110 (m); 1074 (w); 1032 (w); 1000 (w).

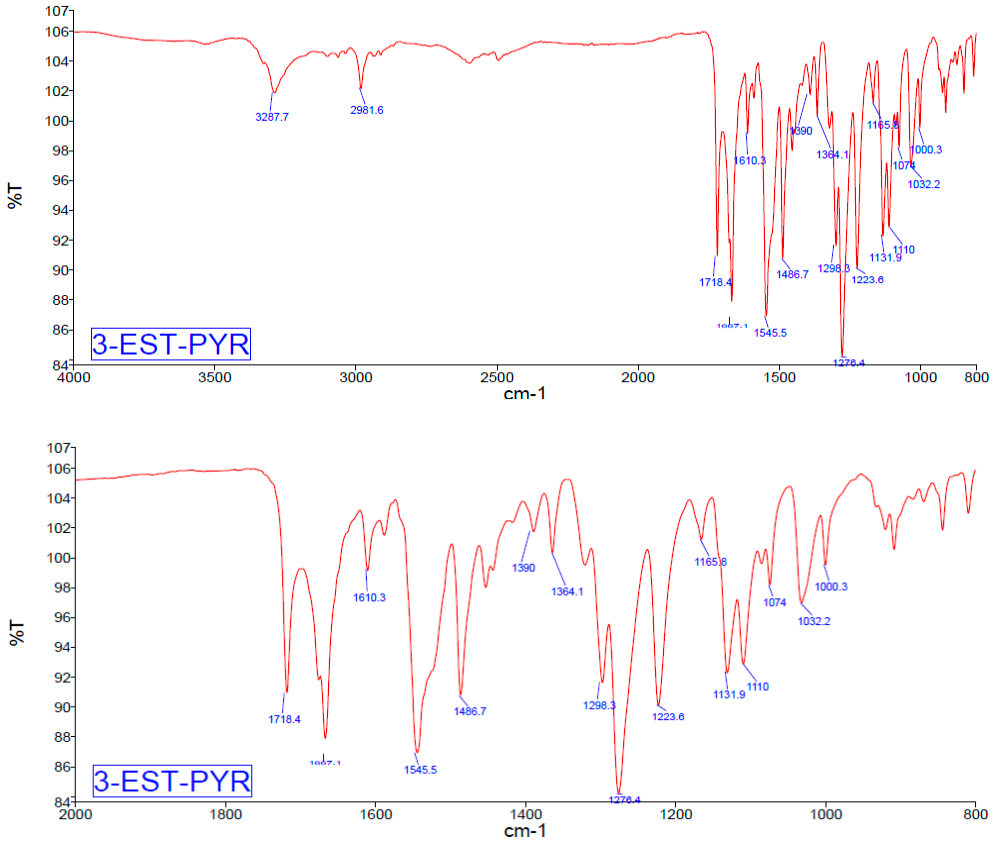

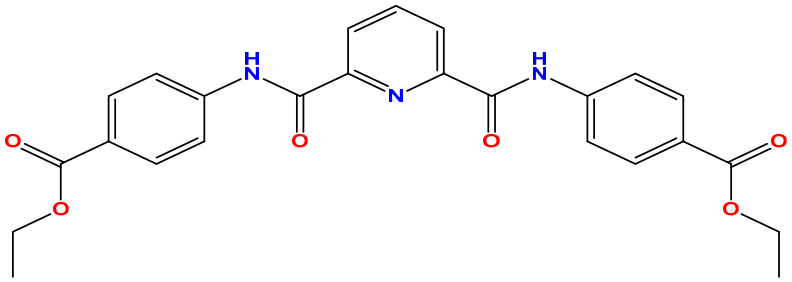

diethyl 4,4'-((pyridine-2,6-dicarbonyl)bis(azanediyl))dibenzoate
Chemical Formula: $C_{25}H_{23}N_3O_6$

6. **P4E** or (4-Est-PYR) (m.p. = 215.0–217.0 °C).

6.1. ^{1}H NMR ($CDCl_3$) δ 1.33 (6H, t, ^{3}J = 7.2 Hz); δ 4.30 (4H, q, ^{3}J = 7.2 Hz); δ 7.77 (4H, d, ^{3}J = 8.6 Hz); δ 8.0 (4H, d, ^{3}J = 8.6 Hz); δ 8.09 (1H, t, ^{3}J = 7.8 Hz); δ 8.43 (2H, d, ^{3}J = 7.8 Hz); δ 9.66 (2H, br s).

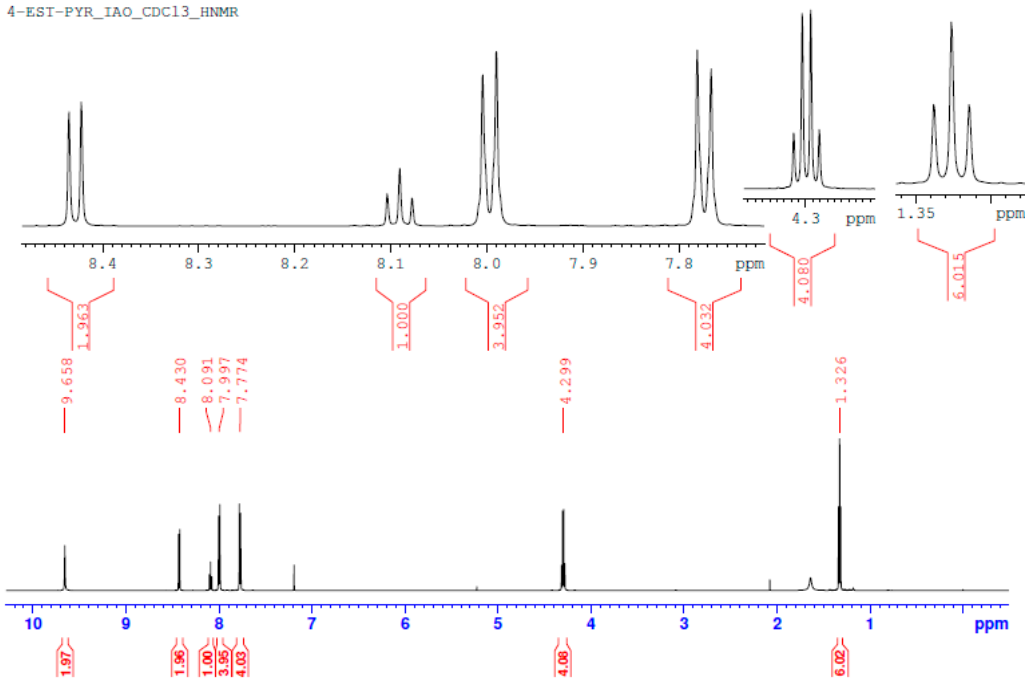

6.2. ^{13}C NMR ($CDCl_3$) δ 14.35; 61.04; 119.45; 126.08; 126.78; 130.91; 139.87; 141.04; 148.74; 161.26; 166.03.

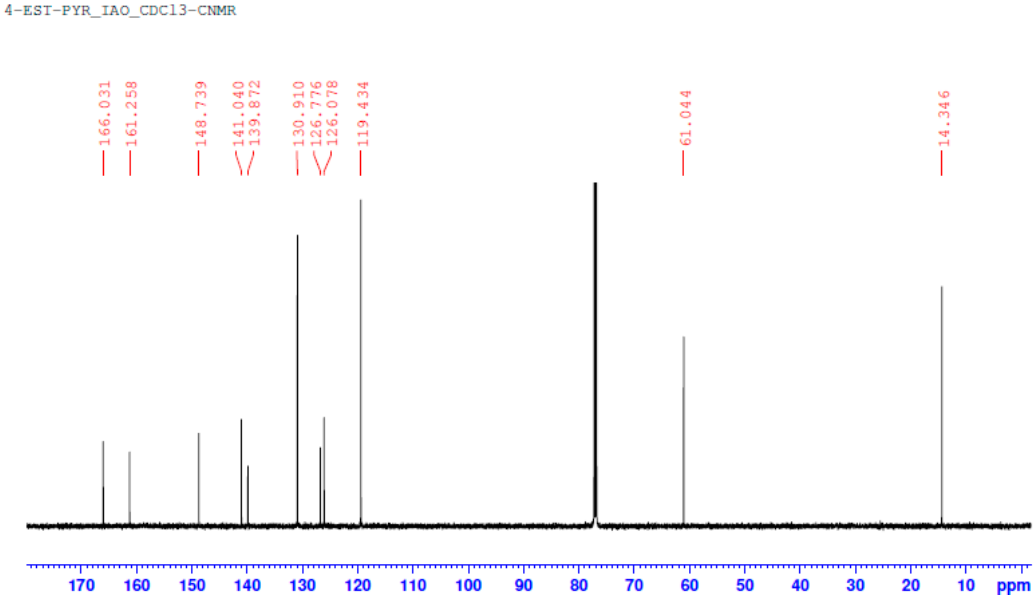

6.3. ATR-IR: 3544 (w); 3290 (w); 2984 (w); 1709 (m); 1690 (m); 1606 (m); 1523 (s); 1408 (m); 1370 (m); 1276 (s); 1176 (m); 1123 (m); 1107 (m); 1017 (m).

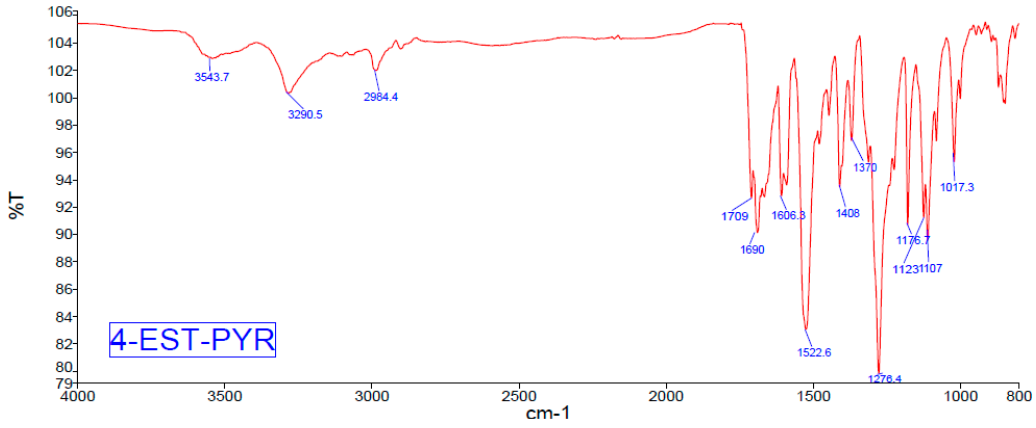

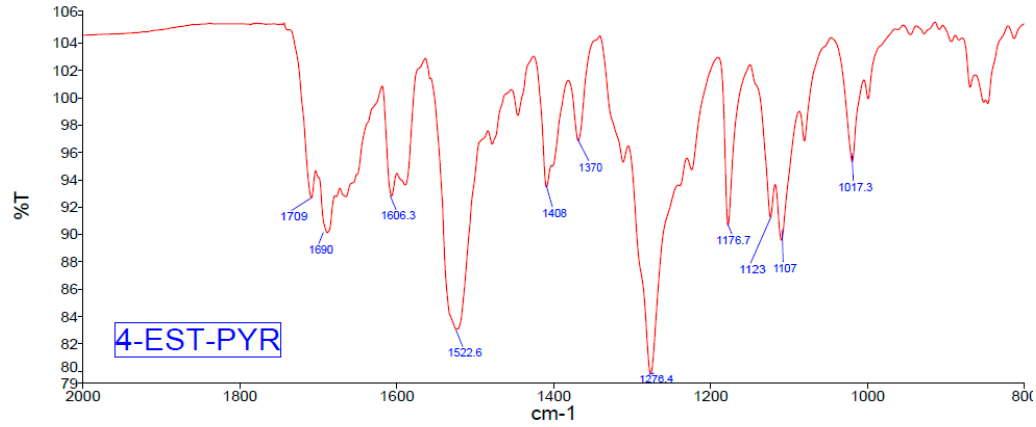

S5. Infrared Spectroscopic Studies of DxE and PxE

The infrared spectra show the important functional groups in the molecular structures and can reveal intermolecular forces. In general, all **DxE** and **PxE** compounds show medium peaks at 3500–3100 cm^{-1} for the N–H-bond stretch. All spectra of the six diamides have strong peaks at 1700–1650 cm^{-1} for the C=O-bond stretch, as would be expected.

Whereas all **PxE** spectra show the presence of water molecules in their crystal structures, the **DxE** spectra lack the water of crystallisation in their structures and appear to be dry, except for **D2E**, which has a broad peak at 3500–3100 cm^{-1} (perhaps a slightly wet sample?), although the crystal structure did not incorporate any water molecules. This broad peak could be due to the formation (O···H) of intramolecular hydrogen bonding (**IMHB**), which can also be verified by the decrease in the carbonyl group wavenumbers from 1710 cm^{-1} (in the other molecules) to 1678 and 1677 cm^{-1}. Similarly, the **P2E** infrared spectrum shows some peaks that indicate the formation of **IMHB**, such as the weak stretch peaks of (O···H) at 3641 and 3471 cm^{-1} and the two medium and weak peaks for N–H at 3338 and 3187 cm^{-1}, respectively.

^{1}H NMR comparison diagram for PxE (top three plots) and DxE (bottom three plots): an overlap plot of the ^{1}H NMR aromatic region for the six **PxE** and **DxE** compounds in $CDCl_3$: ^{1}H-NMR spectra of **x-Est-PYR** (**PxE**) and **x-Est-DIP** (**DxE**) in $CDCl_3$.

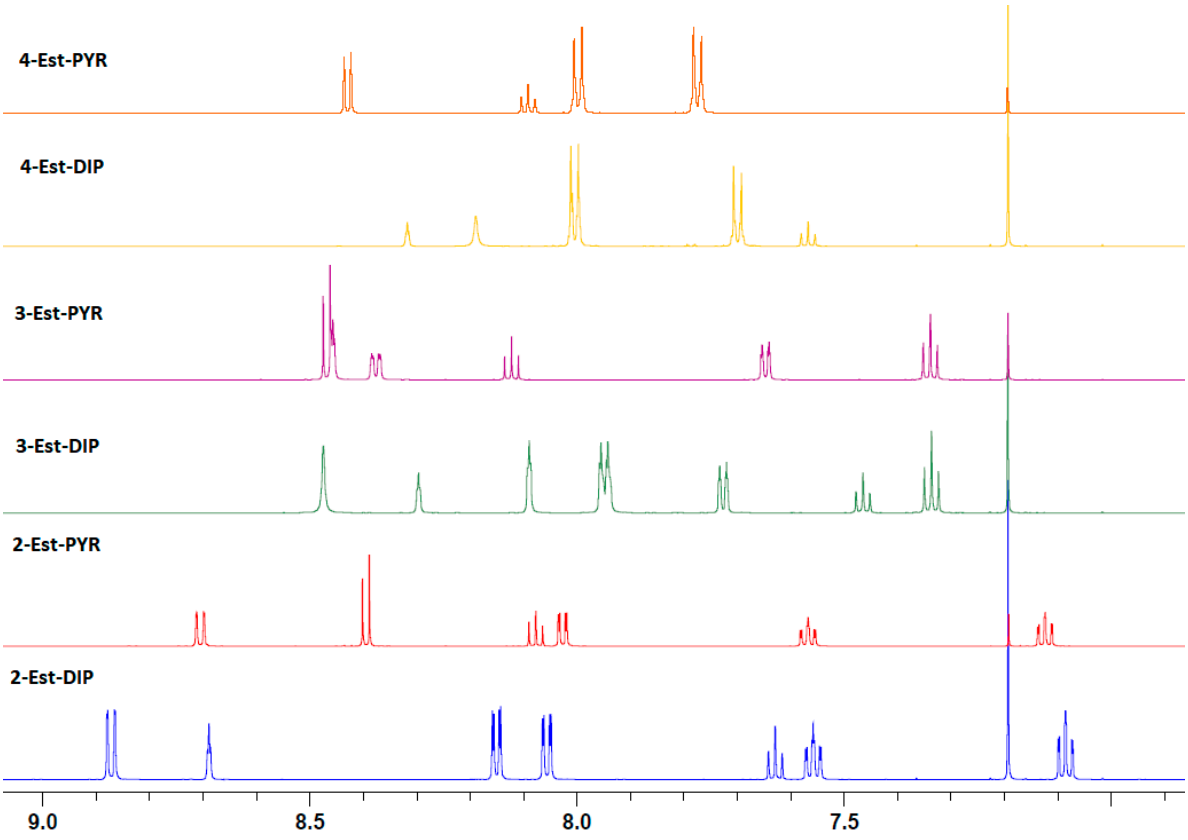

The long nomenclature form as **x-Est-PYR** (for **PxE**) and **x-Est-DIP** (for **DxE**) is used in the diagram above. This is shortened in the manuscript text for brevity. Both naming systems are interchangeable, although **PxE** and **DxE** are mostly retained for brevity.

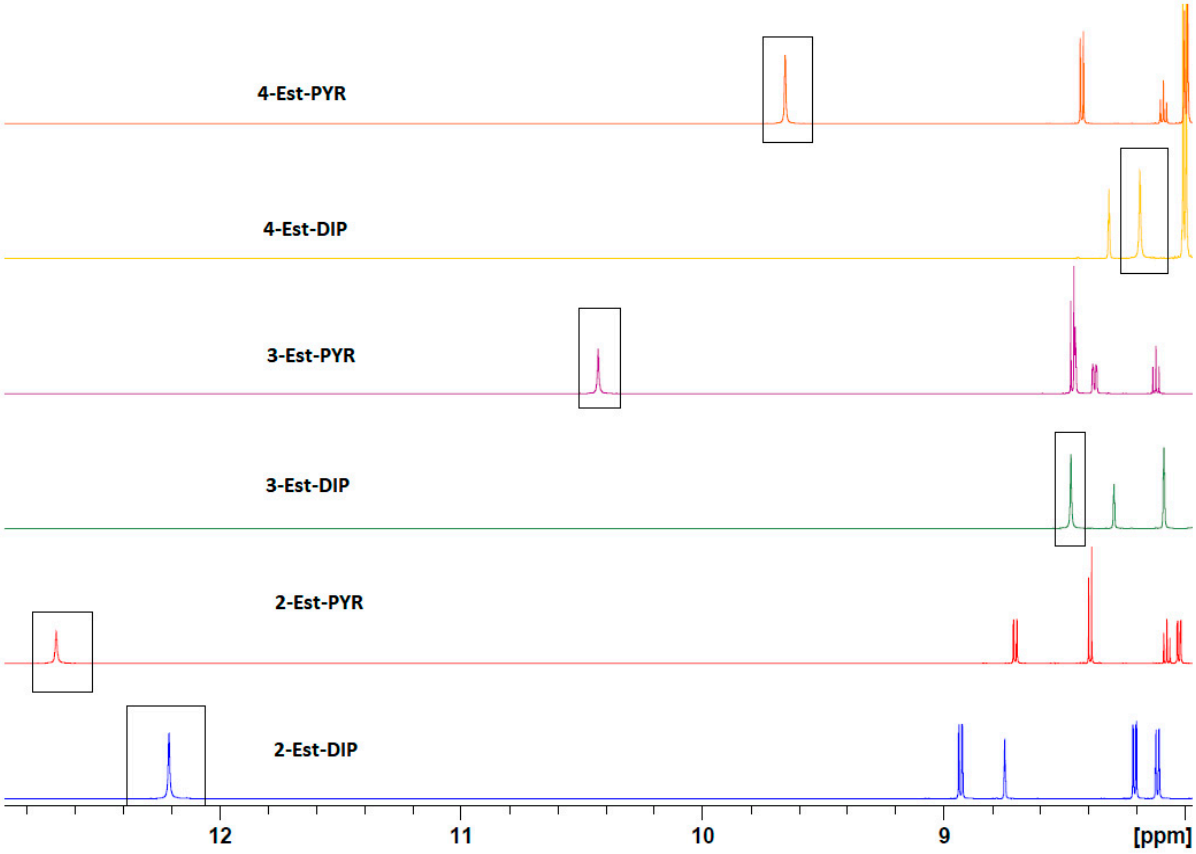

^{1}H-NMR spectra of x-Est-PYR (**PxE**) and x-Est-DIP (**DxE**) ($CDCl_3$; N–H chemical shift highlighted).

The chemical shifts of the amide group protons are worthy of discussion, with the chemical shift of the N–H proton in $CDCl_3$ from 8.5 to 9.5 ppm. The **3-Est-DIP (D3E)** and **4-Est-DIP** (**D4E**) isomers show quite predictable chemical shifts at 8.47 and 8.19 ppm, respectively (^{1}H NMR spectral comparisons above), while the **3-Est-PYR** (**P3E**) and **4-Est-PYR** (**P4E**) isomers show slight increases in their chemical shifts to 10.44 and 9.66 ppm, respectively, which can be explained by the effect of the central pyridine group instead of the benzene ring. In contrast, the *ortho*-substituted **2-Est-DIP** (**D2E**) and **2-Est-PYR** (**P2E**) exhibit substantial increases in their chemical shifts to 12.15 and 12.68 ppm, respectively (^{1}H NMR above). This downfield chemical shift is due to the proximity of the N–H group to the ester carbonyl groups and the formation of intramolecular hydrogen bonding (IMHB) in (**P2E**) and (**D2E**). The ^{13}C NMR spectra for all six **PxE** and **DxE** compounds are as expected and detailed in the spectroscopic data section.

S6. Melting-Point Details and Summary for DxE and PxE

The melting-point measurements for the two sets of three **DxE** and **PxE** isomers display high melting-point ranges, as noted specifically for **DxE** (**Table S1**). Both isomer grids have symmetrical structures, which plays a role in the observed melting points. The **DxE** isomers have a higher melting-point range than the **PxE** isomers, although the presence of the pyridine ring in **PxE** was expected to increase the melting range. The effect may be due to the presence of water molecules in the **PxE** structures with **P3E** and **P4E** as dihydrates.

The melting range of each group follows Carnelley's rule for symmetrical structures and thermodynamic factors. The *meta*-substituted isomers (**D3E** and **P3E**) have the lowest melting points, as they are the least symmetrical. Based on the crystal structures, the **D3E** structure is the least symmetrical, which may explain its low melting point compared with those of the other **DxE** isomers. The *ortho*-substituted isomers (**D3E** and **P3E**) have higher melting points than the *meta*-substituted isomers. Finally, the *para*-substituted isomers (**D4E** and **P4E**) exhibit the highest melting ranges. The generally lower melting ranges of the **PxE** compounds might be explained by the presence of water molecules incorporated within the **PxE** structures, as seen in their infrared spectra and crystal structures, although the melting-point measurements were performed on pure powder samples and not on single crystals. Moreover, in contrast, the crystal structures of the three **DxE** isomers contain no water molecules. The presence of water molecules may restrict the intermolecular interactions between the **PxE** molecules; hence, the major interactions are hydrogen bonds (as C=O···H–O, N–H···O–H) with the water molecule, which is displaced or evaporates from the crystals at a lower temperature than that for the related **DxE** systems.

Melting-point ranges of the **DxE** and **PxE** compounds.

Isomer	Melting-Point Range (°C)	Isomer	Melting-Point Range (°C)
D2E	204–206	**P2E**	177–179
D3E	172–174	**P3E**	172–174
D4E	238–240	**P4E**	215–217

Table S1. a. Experimental details for the DxE structure triad. Experiments performed at 100 (1) K with Cu *K*a radiation using an XtaLAB Synergy, Dualflex, AtlasS2 for **DxE**.

Crystal Data	**D2E**	**D3E**	**D4E**
Chemical formula	$C_{26}H_{24}N_2O_6$	$C_{26}H_{24}N_2O_6$	$C_{26}H_{24}N_2O_6$
M_r	460.47	460.47	460.47
Crystal system, space group	Monoclinic, *C*2/*c*	Monoclinic, $P2_1$	Monoclinic, $P2_1/c$
a, *b*, *c* (Å); *β* (°)	16.8021 (12), 17.2770 (13), 7.5772 (10) Å; 101.51 (1)°	4.6930 (1), 47.4327 (16), 20.0714 (7) Å; 90.447 (3)°	45.2027 (10), 5.0879 (1), 9.7151 (2) Å; 93.245 (2)°
V (Å^3)	2155.4 (4)	4467.8 (2)	2230.76 (8)
Z, *Z*′	4, 0.5	8, 4	4, 1
F(000)	968	1936	968
D_x (Mg m^{-3})	1.419	1.369	1.371
Cell measurement reflections	976	17293	18,401
μ (mm^{-1})	0.84	0.81	0.81
Crystal shape; colour	Needle; colourless	Needle; colourless	Plate; colourless
Crystal size (mm)	0.26 × 0.02 × 0.01	0.27 × 0.05 × 0.02	0.21 × 0.13 × 0.01
Data collection			
Absorption correction	Multi-scan; ABSPACK	Gaussian, *CrysAlis PRO* 1.171.39.27b, 2015	Multi-scan, *CrysAlis PRO* 1.171.38.43, 2015
T_{min}, T_{max}	0.914, 1.000	0.742, 1.000	0.638, 1.000
Measured; independent; observed reflections ($I > 2\sigma(I)$)	3821; 3821; 2534	50,173; 16,045; 14,317	63,940; 4640; 4414
R_{int}	0.032	0.073	0.071

$\theta_{max/min}$ values (°)	76.7–3.7	76.7–3.7	76.7–3.9
Ranges of *h*, *k*, *l*	*h* = −20⊚21; *k* = −21⊚21; *l* = −5⊚9	*h* = −5⊚4; *k* = −46⊚59; *l* = −25⊚25	*h* = −56⊚57; *k* = −6⊚6; *l* = −10⊚11
Refinement			
$R[F^2 > 2\sigma(F^2)]$; $wR(F^2)$; *S*	0.032; 0.070; 0.81	0.077; 0.207; 1.02	0.079; 0.186; 1.10
Reflections; parameters; restraints	3821; 162; 0	16,045; 1235; 1	4640; 320; 0
H-atom treatment	Independent and constrained refinement	H-atom parameters constrained	Independent and constrained refinement
$\Delta\rho_{max}$, $\Delta\rho_{min}$ (e Å^{-3})	0.25, −0.20	0.39, −0.32	0.40, −0.32
Absolute structure; parameter	–	Flack x determined using 4561 quotients; −0.06(18)	–

D3E: Flack x from 4561 quotients [(I+)-(I-)]/[(I+)+(I-)] (Parsons, Flack and Wagner, *Acta Cryst*. **B69** (2013) 249–259).

Table S1b. Experimental details for the PxE structure triad. Experiments performed at 100(1) K with Cu *Ka* radiation using an XtaLAB Synergy, Dualflex, AtlasS2 for **PxE**. H atoms treated by a mixture of independent and constrained refinement for all three **PxE** isomers.

Crystal Data	**P2E**	**P3E**	**P4E**
Chemical formula	$C_{25}H_{23}N_3O_6 \cdot 0.441(H_2O)$	$C_{25}H_{23}N_3O_6 \cdot 2(H_2O)$	$C_{25}H_{23}N_3O_6 \cdot 2(H_2O)$
M_r	469.41	497.49	497.49
Crystal system, space group	Monoclinic, $P2_1/n$	Monoclinic, $I2/a$	Monoclinic, $P2_1/c$
a, b, c (Å); β (°)	10.2905 (2), 6.9758 (1), 30.4312 (5) Å; 94.8700 (15)°	13.9902 (2), 11.8390 (1), 28.2817 (3) Å; 93.863 (1)°	17.2313 (2), 6.8900 (1), 20.2513 (3) Å; 104.7166 (14)°
V (Å^3)	2176.60(6)	4673.65(9)	2325.43(6)
Z, Z'	4, 1	8, 1	4, 1
$F(000)$	985.6	2096	1048
D_x (Mg m^{-3})	1.432	1.414	1.421
No. of reflections for cell measurement	4983	9393	16,669
μ (mm^{-1})	0.87	0.89	0.90
Crystal shape; colour	Lathe; colourless	Block; colourless	Rod; colourless
Crystal size (mm)	0.14 × 0.10 × 0.02	0.14 × 0.10 × 0.06	0.22 × 0.06 × 0.03
Data collection			
Absorption correction	Gaussian; *CrysAlis PRO* 1.171.39.27b, 2015	Gaussian; *CrysAlis PRO* 1.171.39.27b, 2015	Gaussian; *CrysAlis PRO* 1.171.39.27b, 2015
T_{min}, T_{max}	0.830, 1.000	0.847, 1.000	0.817, 1.000
Measured; independent; observed reflections $I > 2\sigma(I)$	8961; 4417; 3970	14,517; 4838; 4484	54,318; 4852; 4011
R_{int}	0.016	0.012	0.052
$\theta_{max/min}$ values (°)	76.7–4.4	76.6–4.1	76.3–4.5
Ranges of h, k, l	$h = -12 \circledcirc 11$; $k = -7 \circledcirc 8$; $l = -31 \circledcirc 38$	$h = -17 \circledcirc 16$; $k = -7 \circledcirc 14$; $l = -34 \circledcirc 35$	$h = -21 \circledcirc 21$; $k = -8 \circledcirc 7$; $l = -25 \circledcirc 25$
Refinement			
$R[F^2 > 2\sigma(F^2)]$; $wR(F^2)$; S	0.031; 0.080; 1.05	0.030; 0.082; 1.02	0.039; 0.110; 1.02
Reflections; parameters; restraints	4417; 336; 0	4838; 352; 0	4852; 350; 4
$\circledcirc\rho_{max}$, $\circledcirc\rho_{min}$ (e Å^{-3})	0.27, −0.20	0.28, −0.16	0.32, −0.39

Computer programs: *CrysAlis PRO* 1.171.39.27b (Rigaku OD, 2015); *CrysAlis PRO* 1.171.38.43 (Rigaku OD, 2018); *SHELXL2014/7* (Sheldrick, 2014); *Mercury*. Unit-cell parameter data for **GAPTUP**[9] and **P2E**[present study]. **GAPTUP**[Reference 9]: a = 10.286(2); b = 7.2038(14); c = 30.590(6) Å; V = 2259 Å^3 at 298 K. **P2E**[present study]: a = 10.2905(2); b = 6.9758(1); c = 30.4312(5) Å; and V = 2176.60(6) Å^3 at 100(1) K. Ethyl-2-((((6-((2-(ethoxycarbonyl)phenyl)carbamoyl)pyridin-2-yl)carbonyl)amino)-benzoate•**0.441H$_2$O.**

Table S2. Selected hydrogen-bond parameters for PxE and DxE crystal structures.

D—H···*A*	*D*—H (Å)	H···*A* (Å)	*D*···*A* (Å)	*D*—H···*A* (°)
D2E				
N1—H1···O2	0.91 (2)	1.86 (2)	2.6509 (17)	143.7 (16)
C13—H13···O2	0.95	2.55	3.4555 (18)	161
C26—H26···O1	0.95	2.28	2.9058 (18)	122
D3E				
N1A—H1A···O4A *i*	0.88	2.25	3.034 (9)	149
N1B—H1B···O4B *i*	0.88	2.33	3.065 (9)	141
N1C—H1C···O4C *ii*	0.88	2.30	3.022 (9)	139
N1D—H1D···O4D *ii*	0.88	2.27	3.032 (9)	144
N2A—H2A···O2C	0.88	2.22	2.962 (9)	141
N2B—H2B···O2D *iii*	0.88	2.23	3.004 (10)	147
N2C—H2C···O2A *iii*	0.88	2.20	2.982 (9)	147
N2D—H2D···O2B	0.88	2.20	3.007 (9)	152
C26A—H26A···O1A	0.95	2.37	2.916 (10)	116
C26B—H26B···O1B	0.95	2.35	2.903 (10)	117
C26C—H26C···O1C	0.95	2.36	2.907 (10)	116
C26D—H26D···O1D	0.95	2.32	2.893 (10)	118
C36A—H36A···O4A	0.95	2.40	2.841 (11)	108
C36C—H36C···O4C	0.95	2.29	2.813 (10)	114
C36D—H36D···O4D	0.95	2.33	2.834 (11)	113
D4E				
N1—H1···O1 *iv*	0.89 (5)	2.11 (5)	2.992 (4)	171 (4)
N2—H2···O4 *v*	0.93 (5)	1.99 (5)	2.899 (4)	166 (4)
C4—H7···O2 *vi*	0.98	2.55	3.282 (5)	131
C8—H101···O5 *vii*	0.98	2.45	3.306 (6)	146
C36—H36···O4	0.95	2.39	2.886 (5)	112

Symmetry code(s): For **DxE**: (*i*) $x + 1, y, z$; (*ii*) $x - 1, y, z$; (*iii*) $x, y, z - 1$; (*iv*) $x, y + 1, z$; (*v*) $x, -y + 3/2, z + 1/2$; (*vi*) $x, -y + 3/2, z - 1/2$; (*vii*) $x, -y + 1/2, z - 1/2$; and for **PxE**: (*viii*) $-x + 1/2, y + 1/2, -z + 1/2$; (*ix*) $-x + 1, -y, -z + 1$; (*x*) $-x + 1/2, y - 1/2, -z + 1/2$; (*xi*) $-x - 1/2, y + 1/2, -z + 1/2$; (*xii*) $-x + 1, -y + 1, -z$; (*xiii*) $-x + 1, y - 1/2, -z + 1/2$; (*xiv*) $-x + 1, y + 1/2, -z + 3/2$; (*xv*) $-x + 2, y + 1/2, -z + 3/2$.

Additional symmetry codes (as used in the main-paper discussion): (*xvi*) $x, 1 - y, z - 1/2$; (*xvii*) $2 + x, y, z$; (*xviii*) $-x, -1 - y, 1 - z$; (*xix*) $1 - x, 1/2 + y, 1/2 - z$; ; (*xx*) $-x, -y, 1 - z$; (*xxi*) $-x, 1 - y, 1 - z$; (*xxii*) $x, y - 1, z$.

D—H···*A*	*D*—H (Å)	H···*A* (Å)	*D*···*A* (Å)	*D*—H···*A* (°)
P2E				
N1—H1···O2	0.885 (16)	1.912 (15)	2.6548 (12)	140.5 (13)
N1—H1···N11	0.885 (16)	2.185 (15)	2.6443 (13)	111.8 (12)
N2—H2···O2	0.890 (16)	2.329 (17)	3.1609 (12)	155.7 (13)
C7—H7B···O4 *viii*	0.99	2.57	3.3138 (14)	132
C13—H13···O1 *ix*	0.95	2.36	3.1483 (13)	140
C15—H15···O5 *x*	0.95	2.56	3.4103 (13)	150
C26—H26···O1	0.95	2.27	2.9014 (14)	123
O1W—H2W···O5 *xi*	0.81 (5)	2.02 (5)	2.829 (2)	175 (4)

P3E				
N1—H1···O1W	0.875 (15)	2.220 (15)	3.0348 (11)	154.8 (13)
N2—H2···O1W	0.877 (14)	2.151 (14)	3.0001 (11)	162.8 (12)
C26—H26···O1	0.95	2.23	2.8316 (13)	121
C36—H36···O4	0.95	2.19	2.8193 (13)	123
O1W—H1W···O2W	0.898 (19)	1.830 (19)	2.7274 (11)	177.5 (17)
O1W—H2W···O1 *xii*	0.873 (19)	2.070 (19)	2.8869 (11)	155.6 (16)
O2W—H3W···O2	0.871 (18)	2.010 (18)	2.8402 (11)	159.0 (16)
O2W—H4W···O5	0.883 (18)	1.954 (19)	2.8075 (11)	162.0 (16)
P4E				
N1—H1···O1W	0.879 (19)	2.254 (19)	3.0917 (17)	159.4 (16)
N2—H2···O1W	0.84 (2)	2.18 (2)	2.9654 (17)	154.5 (17)
C22—H22···O1W	0.95	2.40	3.2354 (18)	146
C26—H26···O1	0.95	2.20	2.8225 (18)	122
C32—H32···O4	0.95	2.28	2.8437 (17)	117
C36—H36···O1W	0.95	2.58	3.2532 (18)	128
C36—H36···O2W	0.95	2.49	3.3806 (18)	155
O1W—H2W···O2W	0.835 (16)	2.059 (18)	2.862 (2)	161 (2)
O1W—H1W···O4 *xiii*	0.836 (16)	2.36 (2)	3.0448 (18)	140 (2)
O2W—H3W···O4 *xiv*	0.978 (17)	1.922 (19)	2.8757 (17)	164 (3)
O2W—H4W···O2 *xv*	0.965 (17)	1.809 (18)	2.7604 (16)	168 (3)

S7. Supplementary Structural Diagrams (as Figures S1–S6)

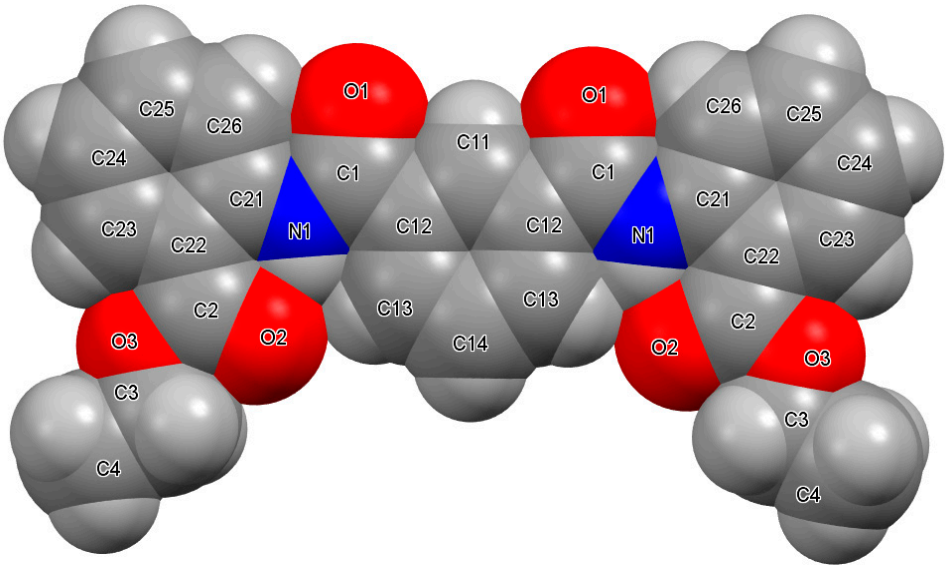

(**a**)

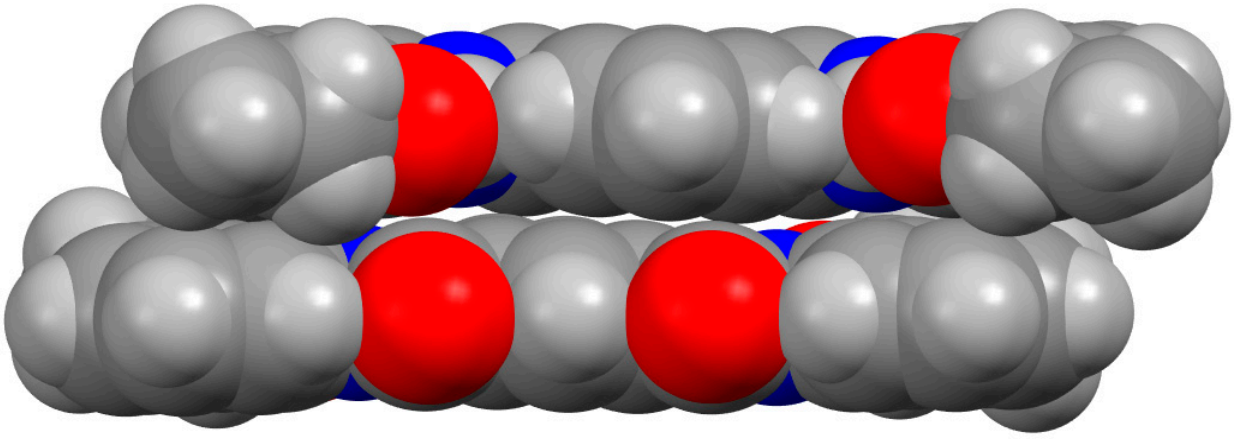

(**b**)

Figure S1. (**a**)The planar **D2E** structure as a CPK model with all nonhydrogen-atom labels. (**b**) **D2E** molecular stacking highlighting the close approach of two planar D2E molecules with closest C…C atom approach of 3.37 Å.

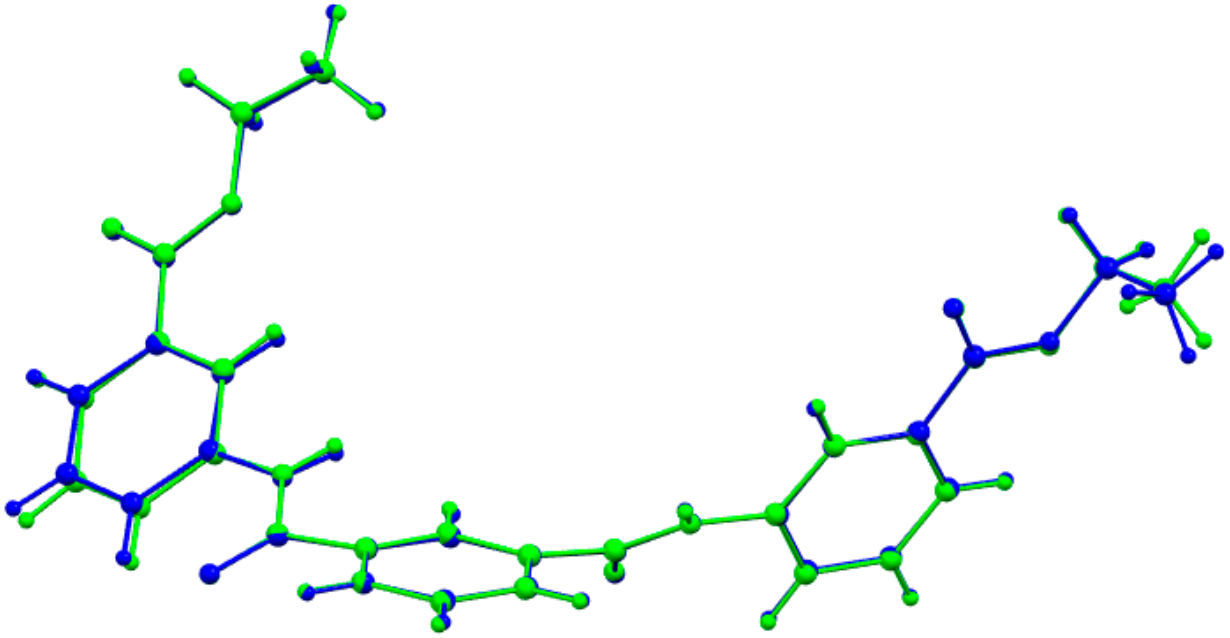

(**a**) Terminal methyl C…C distances are 13.765(17) Å for **C4A**…**C8A** and 13.839(16) Å for **C4B**…**C8B**.

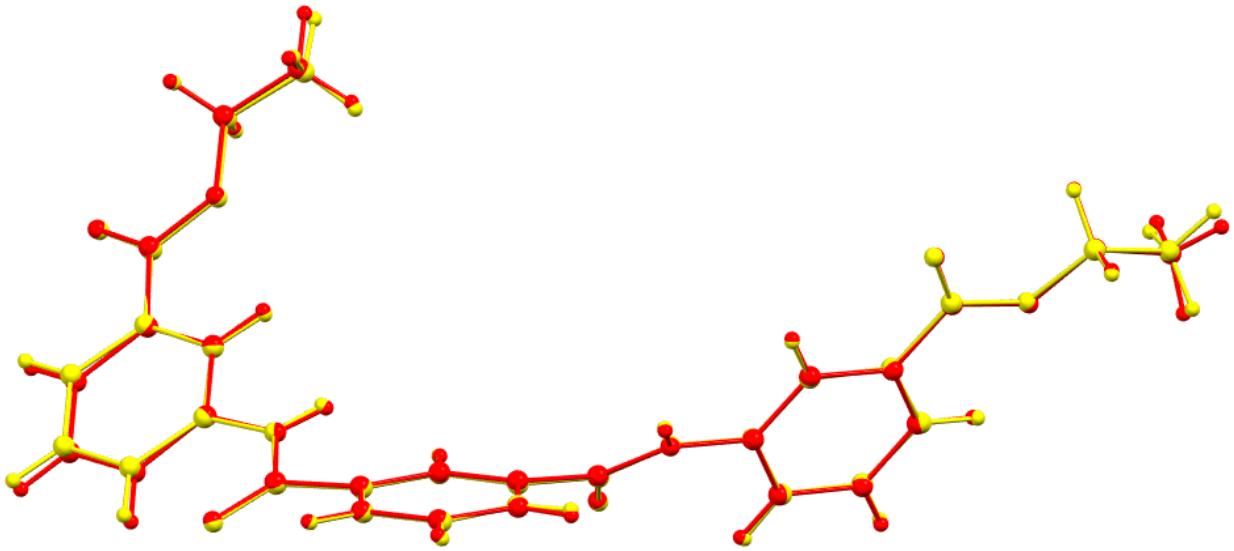

(**b**) Terminal CH_3 C…C distances are 14.325(19) Å for C4C…C8C and 14.230(17) Å for C4D…C8D.

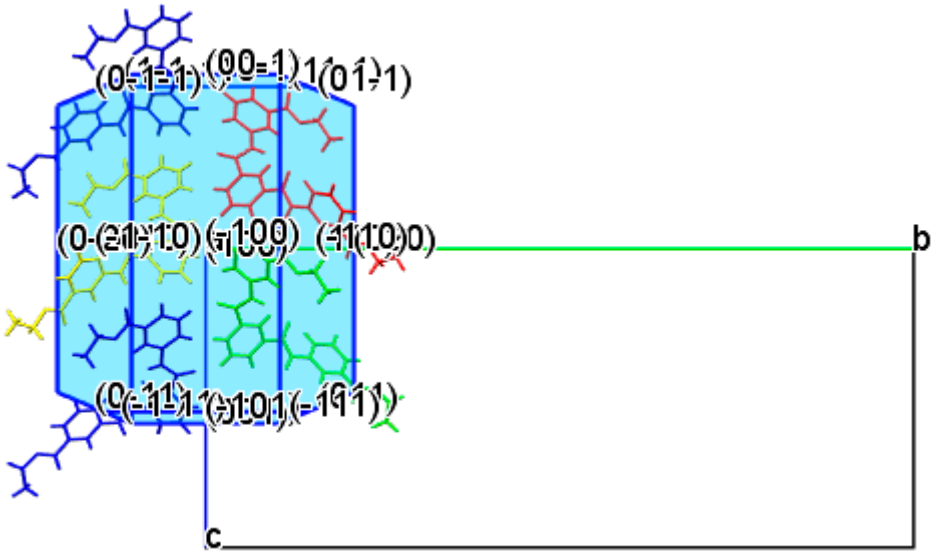

(**c**)

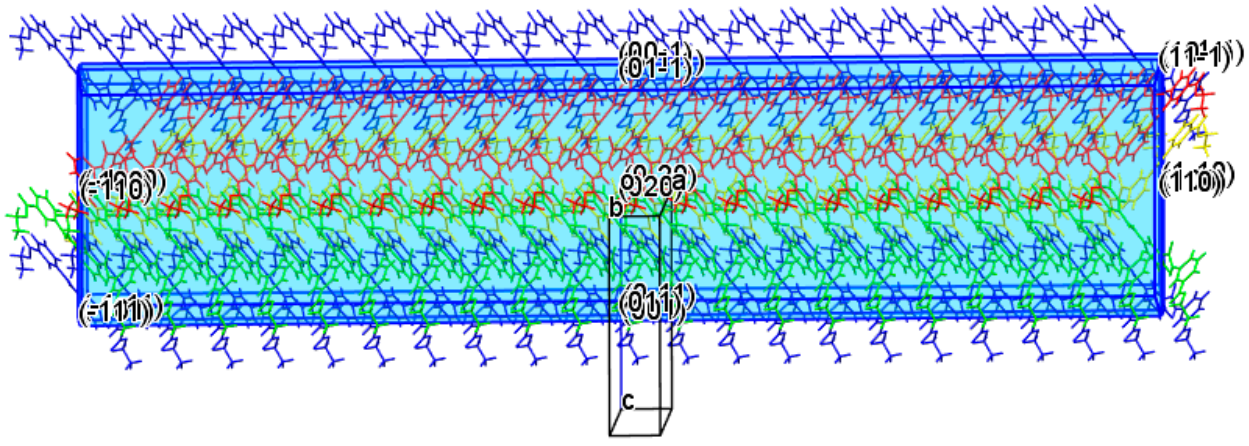

(**d**)

Figure S2. (**a**,**b**) Views of the molecular overlap and overlay of pairs of molecules A–B (**top**) and C–D (**bottom**) in **D3E** highlighting the distinctive pairs formed in the crystal structure. The RMSDs for

the pairs of molecules are 0.07 Å and 0.08 Å, respectively. The interplanar angles for all four sets of C11/C31 rings (middle/right) vary by 8° from 62.5 (3)° (D) to 71.1(3)° (A).(**c**,**d**) Views of **D3E** along the *a*-axis direction and *b*-axis direction (offset). The compact hydrogen bonding and ring…ring stacking propagates in the direction of the long axis of the needle.

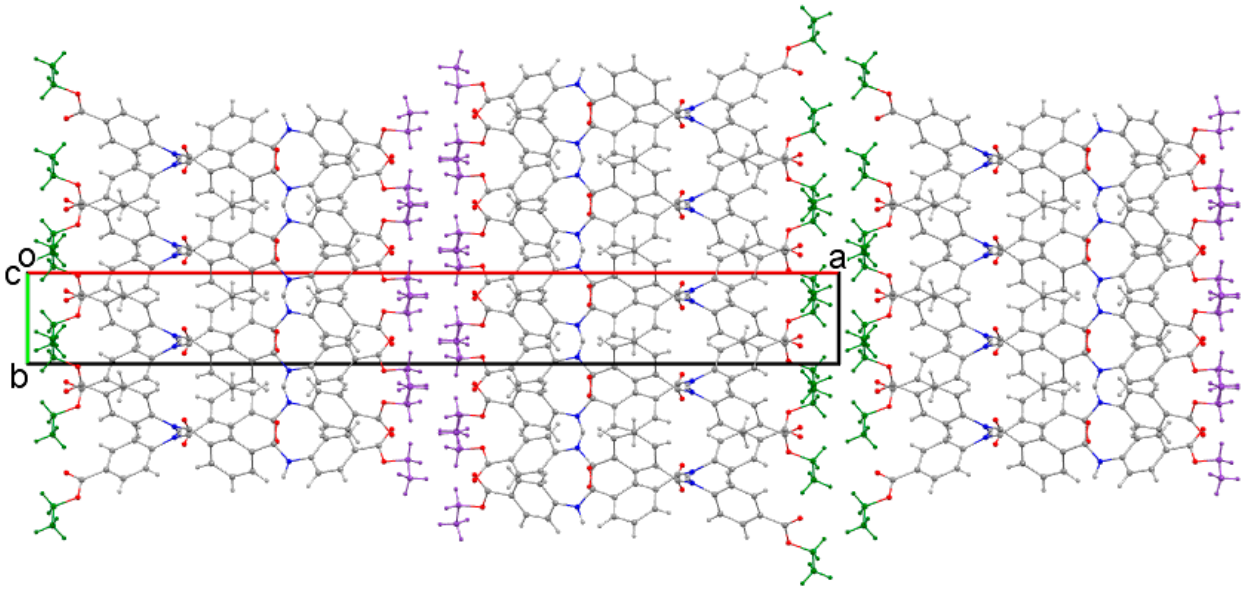

(**a**)

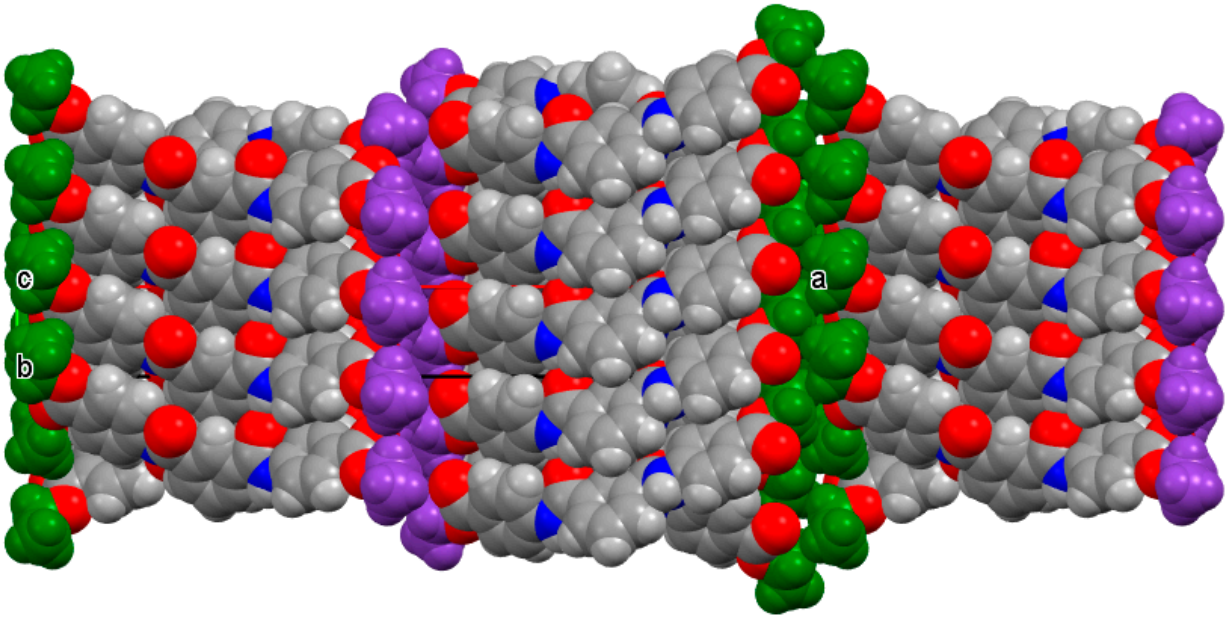

(**b**)

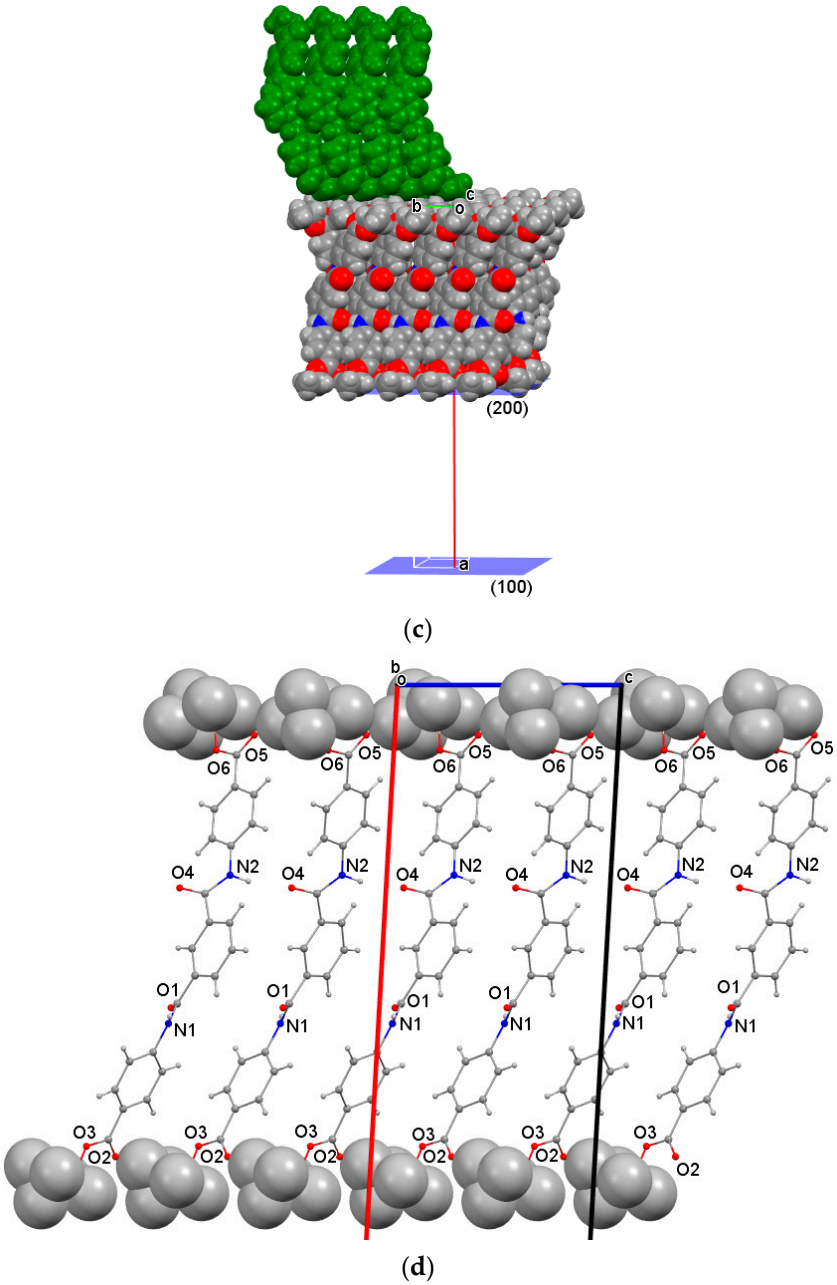

Figure S3. (**a**,**b**) Highlighting of the 2D sheet interfaces on either side of the sheet of **D4E** molecules with one ethyl group (C3–C4) coloured in **purple** and the other (C7–C8) coloured in **green** as a ball-and-stick model and CPK model. (**c**,**d**) CPK view of the molecular sheet in **D4E** formed from the amide…amide interactions with the ethyl group wall at the surface of the sheet interface together with four molecules (in **green**) from an adjacent sheet (left). A snapshot of the layer with atoms depicted as 'ball and stick' and the H atoms of the ethyl ester group that line the interface depicted as their van der Waal spheres (right).

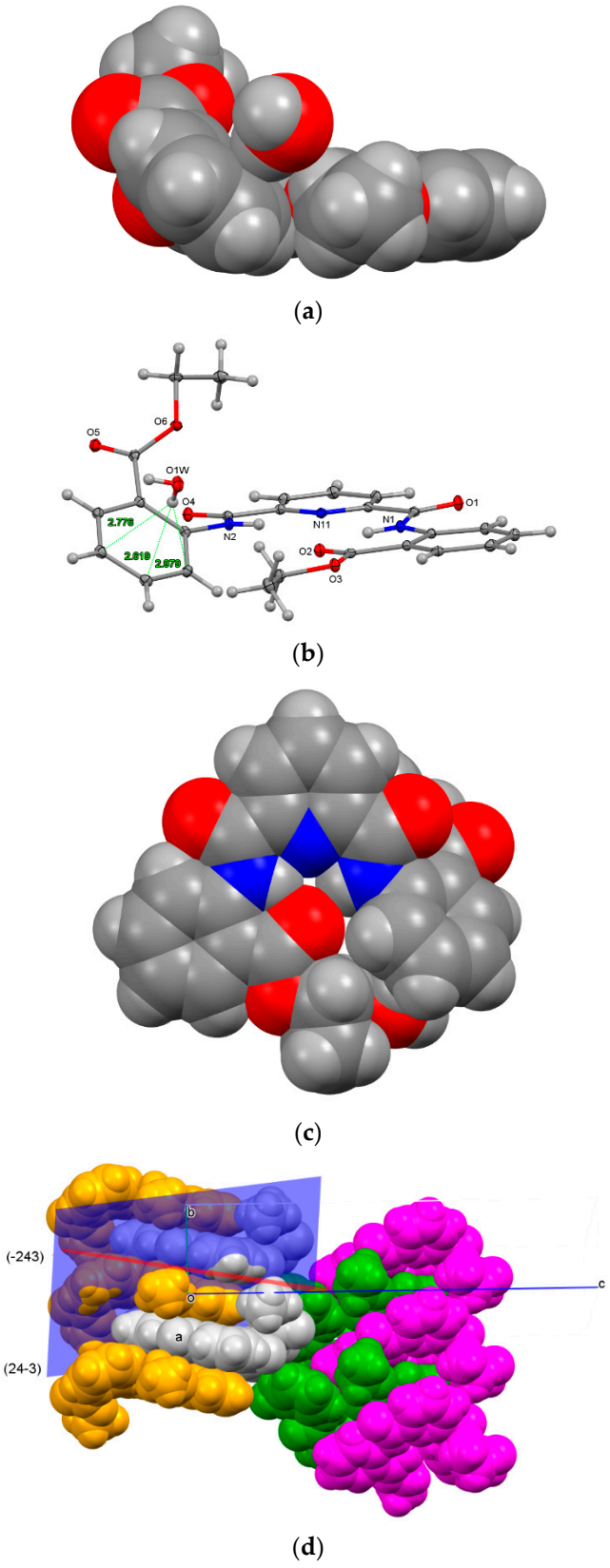

Figure S4. (**a**–**d**) Two views of the O-H…π (arene) interaction in **P2E** (top) and the planar part of **P2E** and the planes through the molecule (bottom).

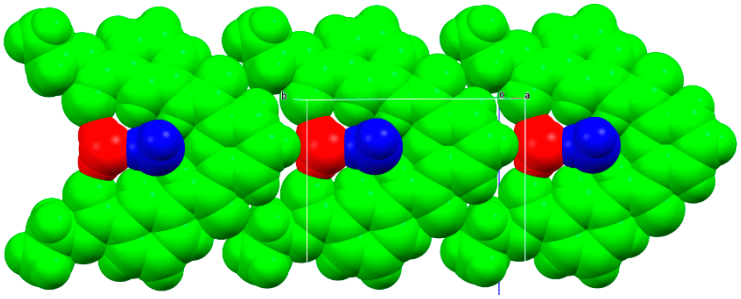

(**a**)

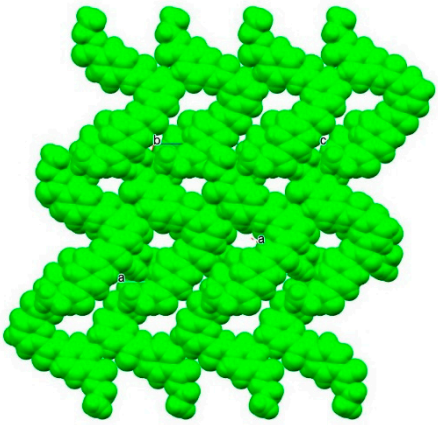

(**b**)

Figure S5. (**a**,**b**) Two CPK views of the **P3E** dihydrate structure showing the arrowhead (water in **red** and **blue**) and a general view with the two water molecules removed.

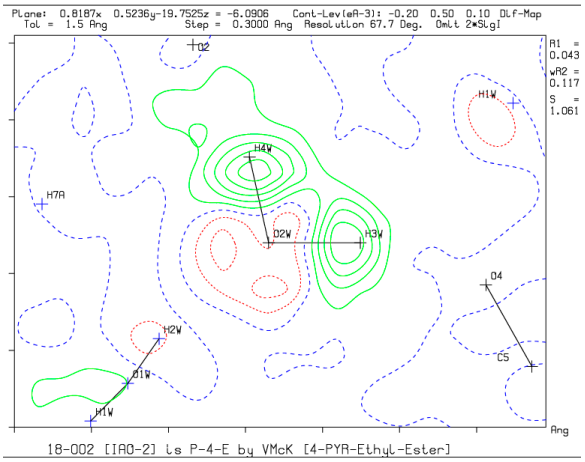
PLane: 0.8187x 0.5236y-19.7525z = -6.0906 Cont-Lev(eA-3): -0.20 0.50 0.10 DLf-Map
Tol = 1.5 Ang Step = 0.3000 Ang Resolution 67.7 Deg. Omit 2*Sig!
R1 = 0.043
wR2 = 0.117
S = 1.061
O2
H1W
H2W
H7A
O2W
H3W
O4
H2W
C5
O1W
H1W
Ang
18-002 [IAO-2] ls P-4-E by VMcK [4-PYR-Ethyl-Ester]

(**a**)

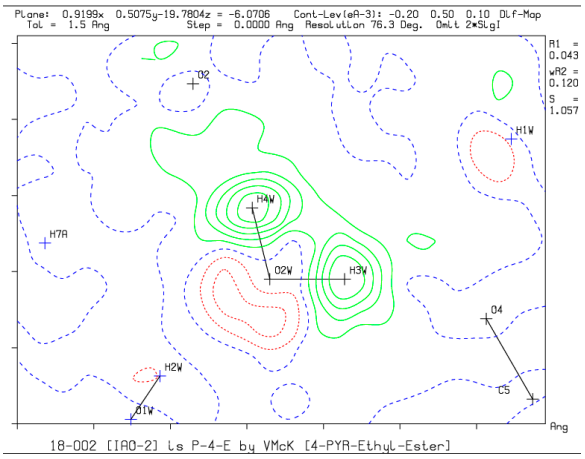
PLane: 0.9199x 0.5075y-19.7804z = -6.0706 Cont-Lev(eA-3): -0.20 0.50 0.10 DLf-Map
Tol = 1.5 Ang Step = 0.0000 Ang Resolution 76.3 Deg. Omit 2*Sig!
R1 = 0.043
wR2 = 0.120
S = 1.057
O2
H1W
H4W
H7A
O2W
H3W
O4
H2W
C5
O1W
Ang
18-002 [IAO-2] ls P-4-E by VMcK [4-PYR-Ethyl-Ester]

(**b**)

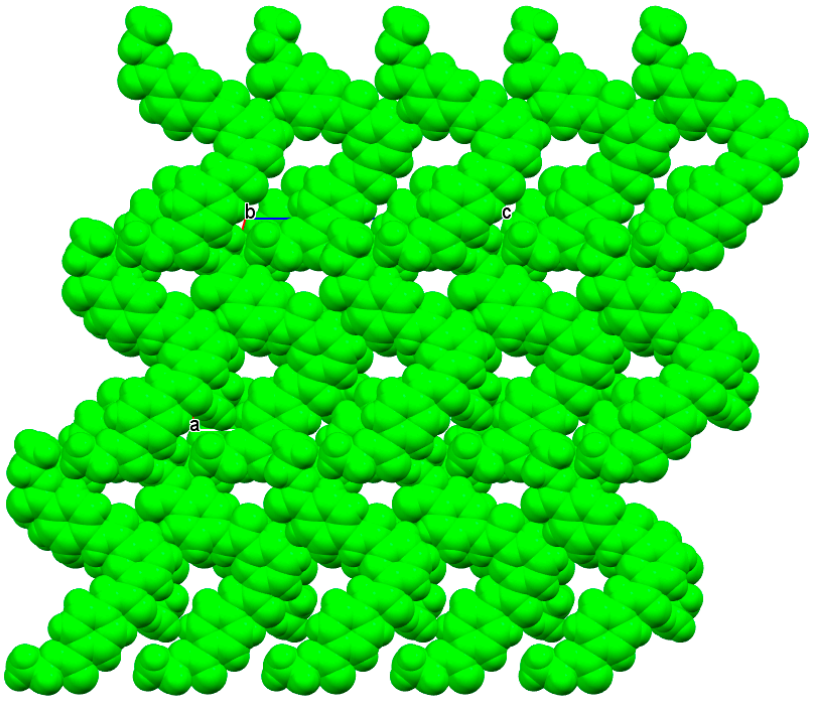
b
c
a

(**c**)

Figure S6. (**a**) Difference Fourier maps of the final refinement cycles in **P4E** without using the DFIX command for the two O2W O-H bonds and (**b**) using a DFIX of 0.85(3) Å for both O-H bonds. The occupancy of the H3W and H4W atoms were set to 0.01 during the PLATON calculation [22]. (**c**) (**1**) Difference map of the O2W molecules (with H occupancy as 0.01) on FMLS refinement to give O-H distances of 1.14 and 1.19 Å, and (**2**) after refinement using DFIX of 0.85 (2) Å to give O-H distances of 0.97 and 0.98 Å; (*c*) CPK view of the **P4E** structure with two water molecules removed (bottom).

S8. Computational Study of the DxE and PxE Molecules (Expanded Plots—Figure S7)

(D2E) or 2-Est-DIP:

Molecular conformations from gas-phase calculations have no direct co-relation with those observed in the solid state. However, the conformational analysis PES diagrams are useful to highlight the similarities and differences between both.

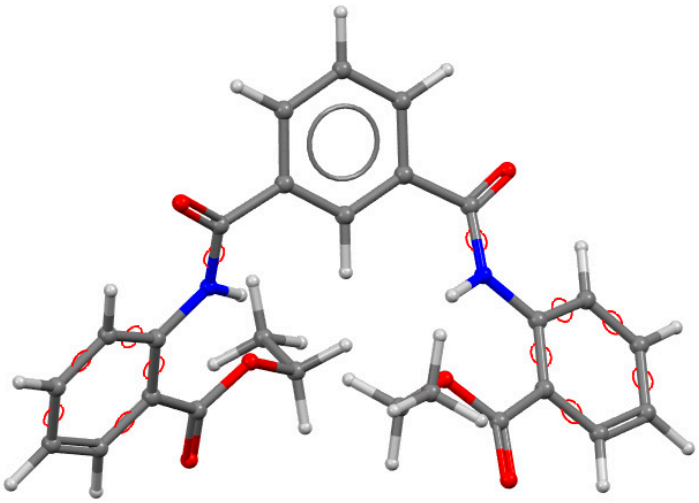

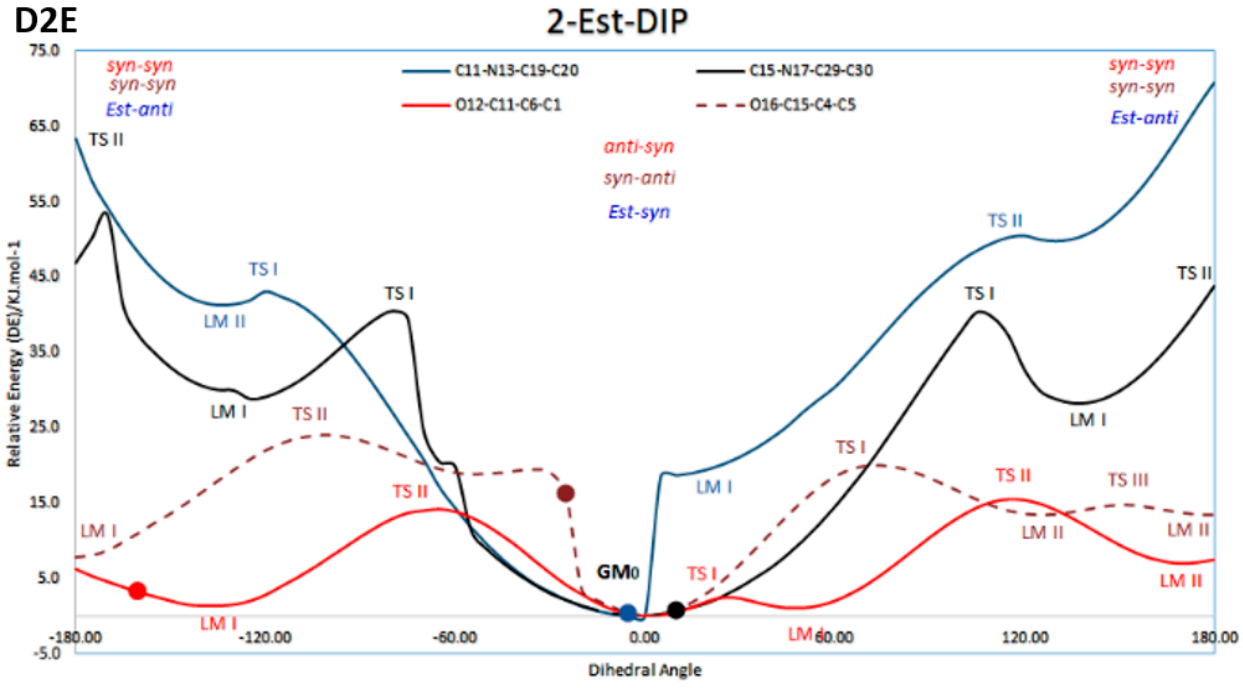

(D3E) or 3-Est-DIP:

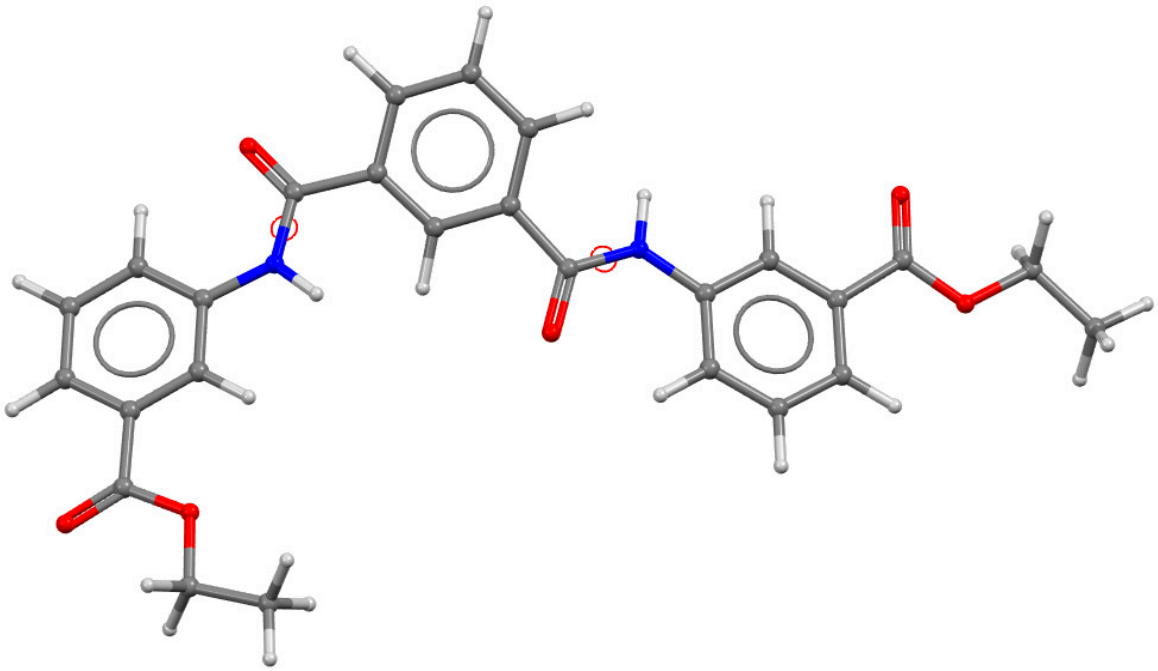

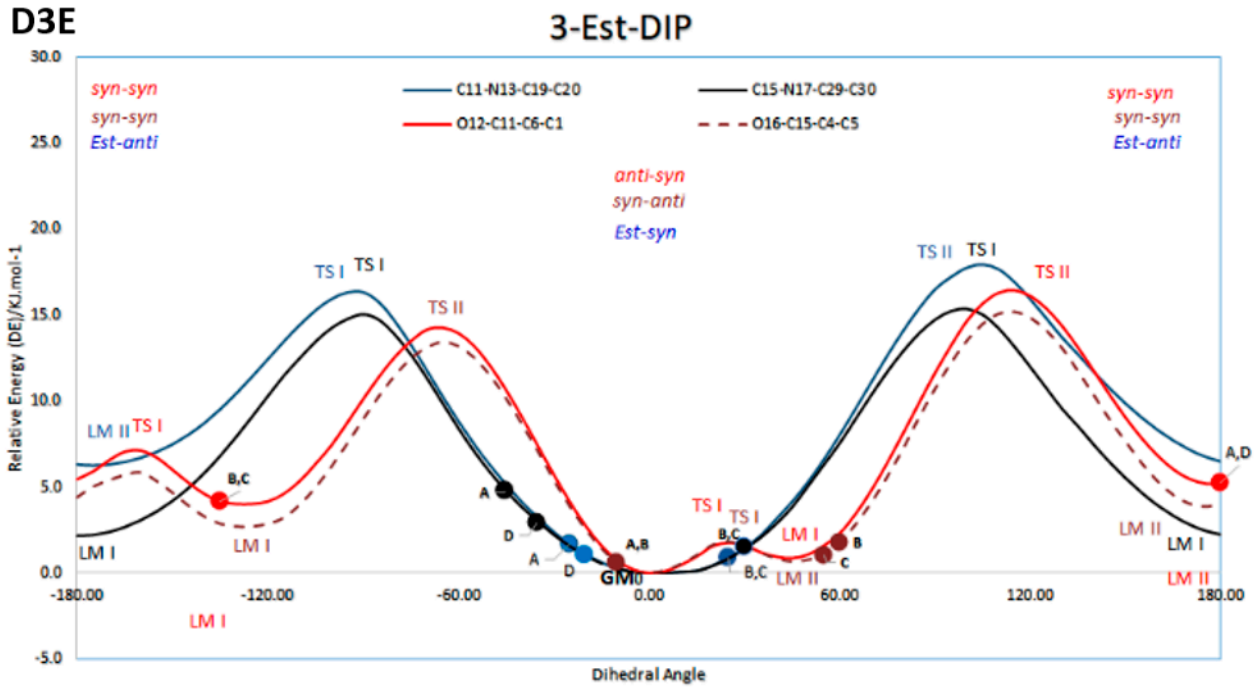

(D4E) or 4-Est-DIP:

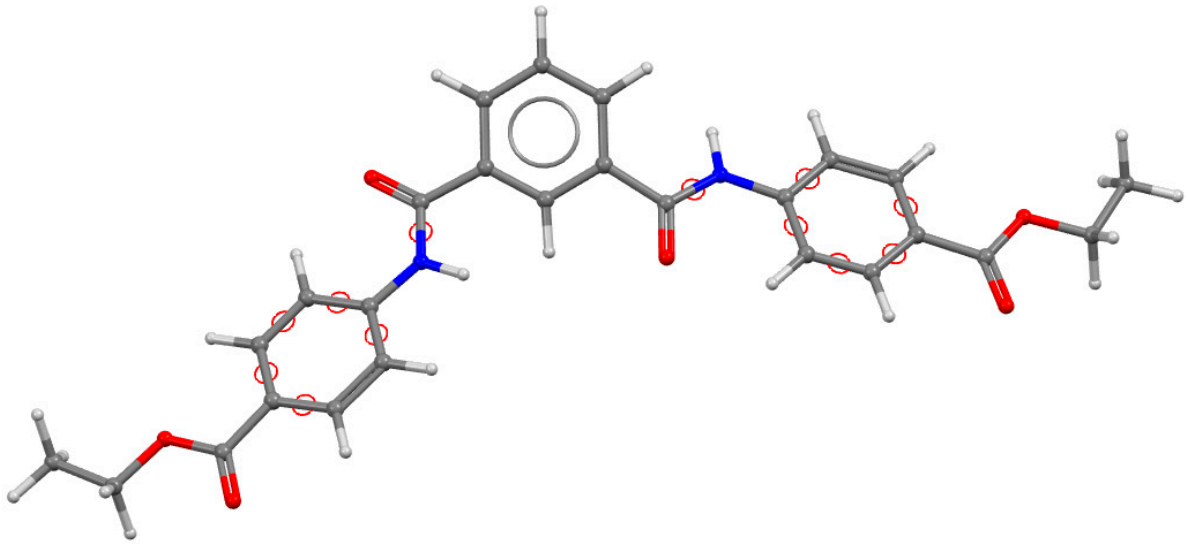

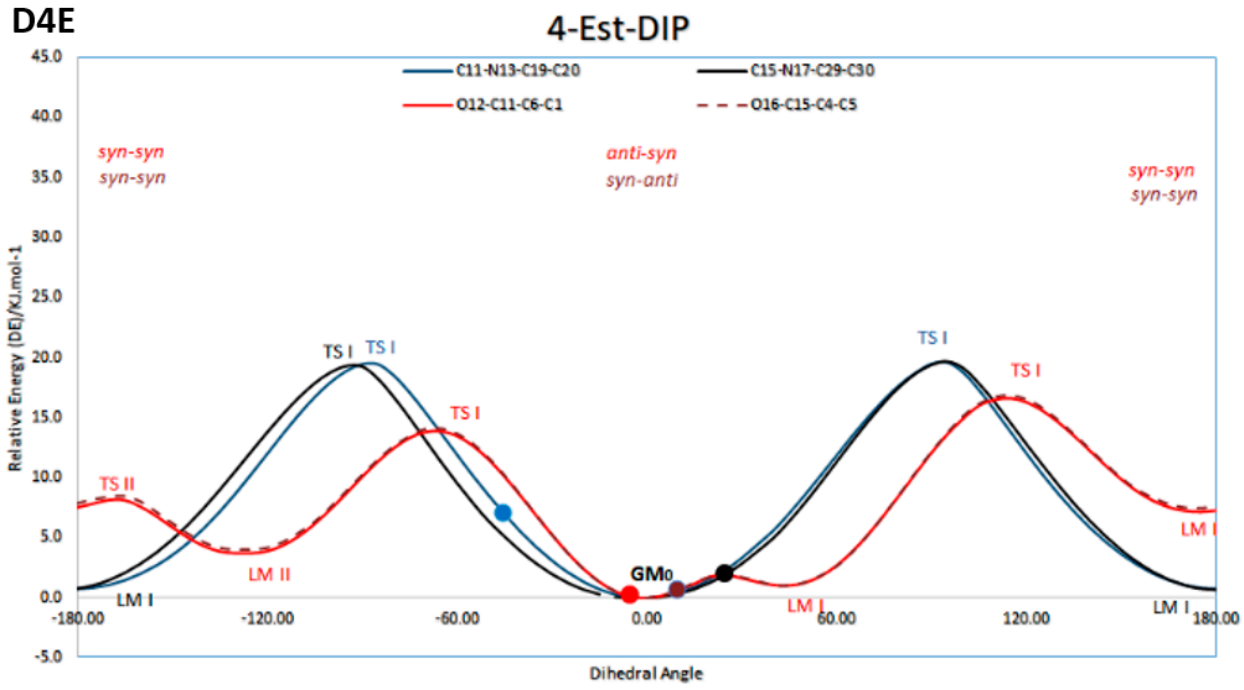

(P2E) or 2-Est-PYR:

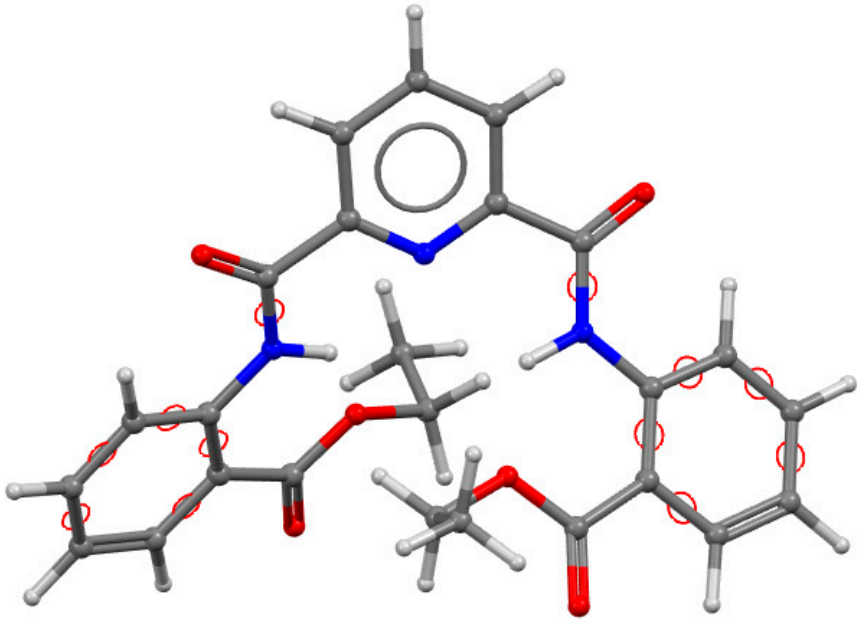

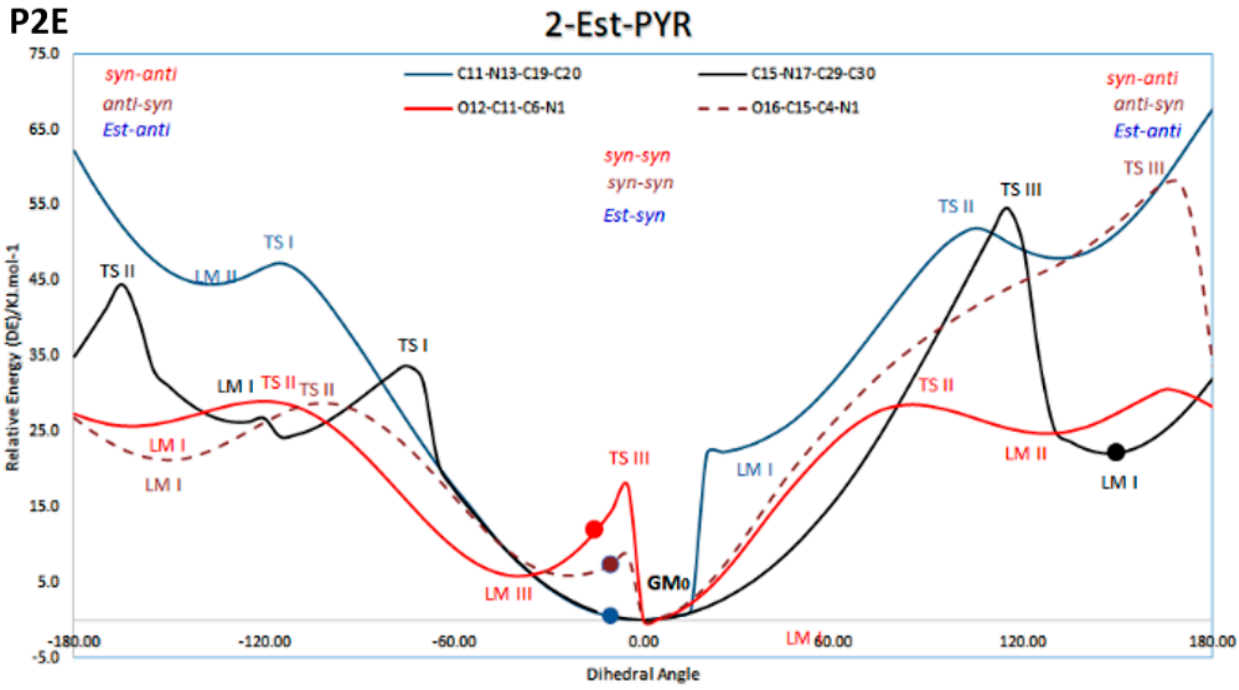
P2E
2-Est-PYR
C11-N13-C19-C20
C15-N17-C29-C30
O12-C11-C6-N1
O16-C15-C4-N1
syn-anti
anti-syn
Est-anti
syn-syn
syn-syn
Est-syn
TS I
TS II
TS III
LM I
LM II
LM III
GM0
Relative Energy (DE)/KJ.mol-1
Dihedral Angle
75.0
65.0
55.0
45.0
35.0
25.0
15.0
5.0
-5.0
-180.00
-120.00
-60.00
0.00
60.00
120.00
180.00

(P3E) or 3-Est-PYR:

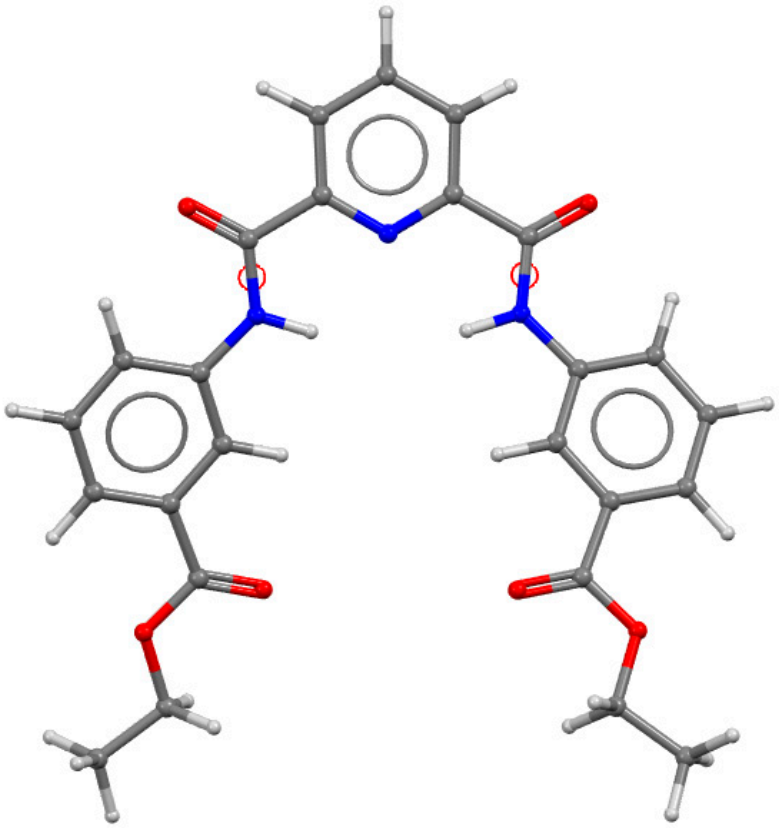

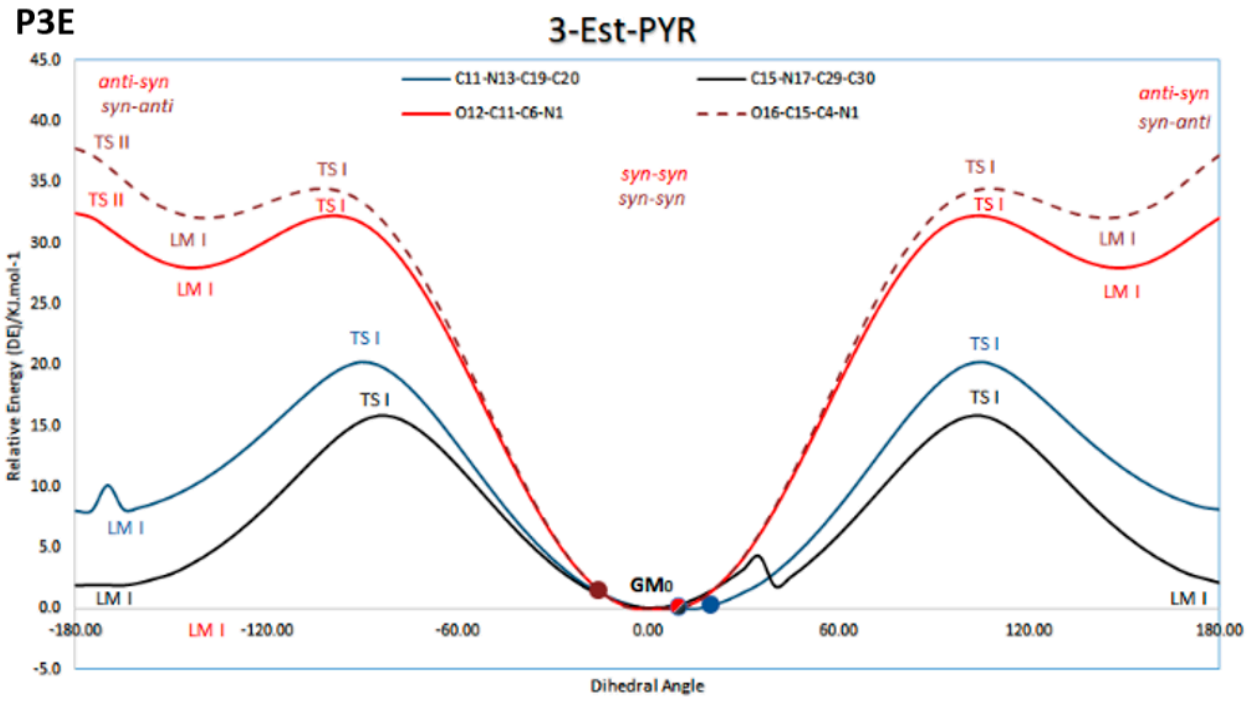

(P4E) or 4-Est-PYR:

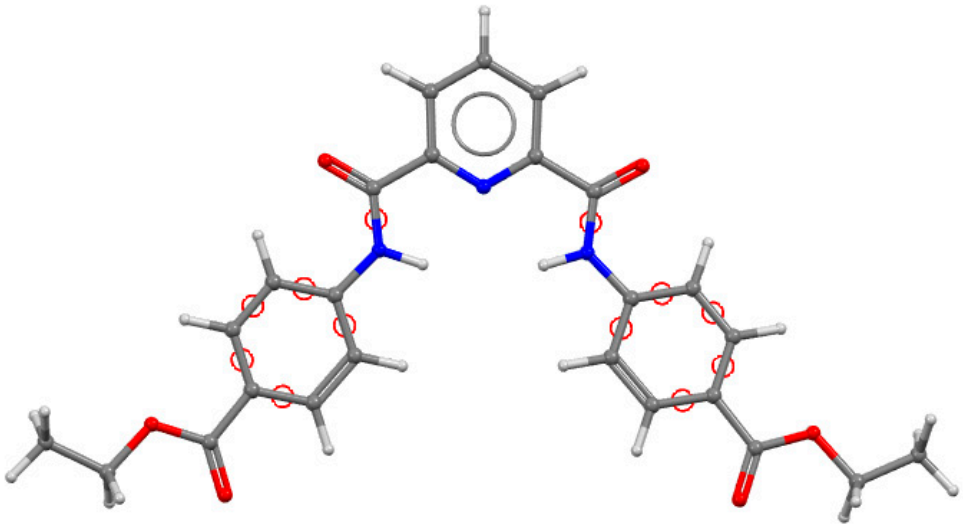

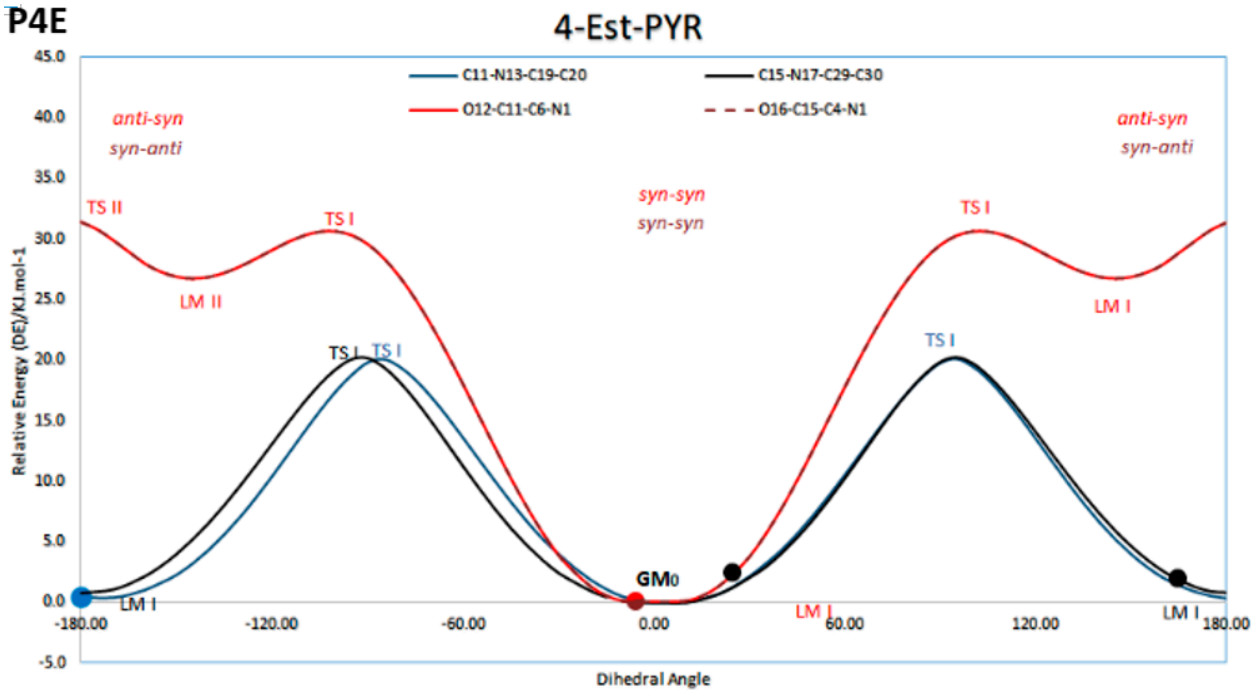

Comparisons (overlap) of the optimised (red) and crystal (blue) structures:

(**D2E**)

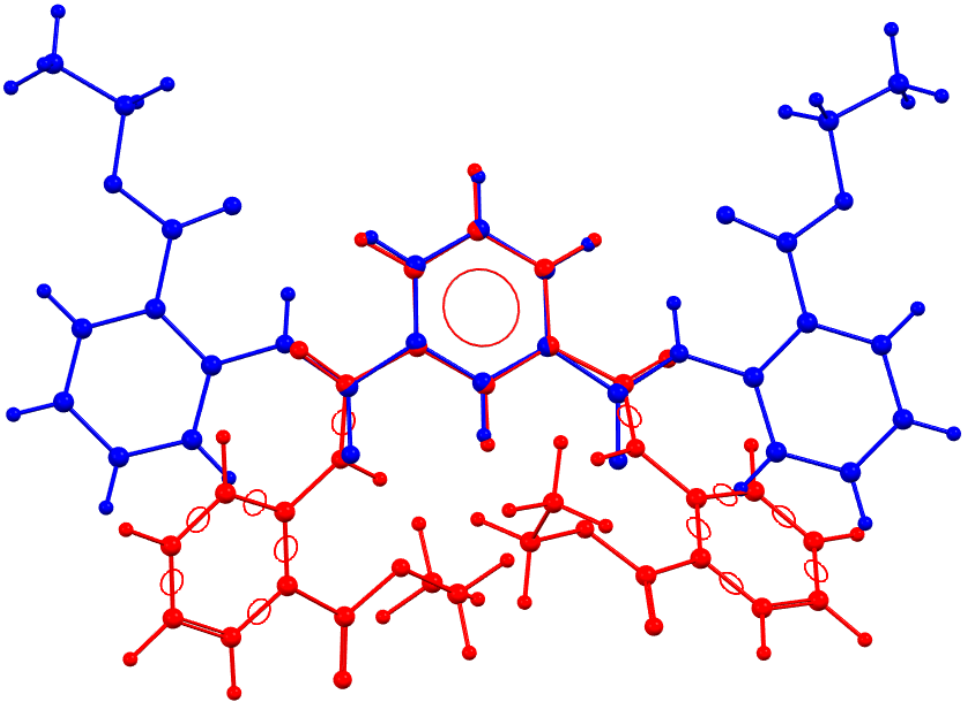

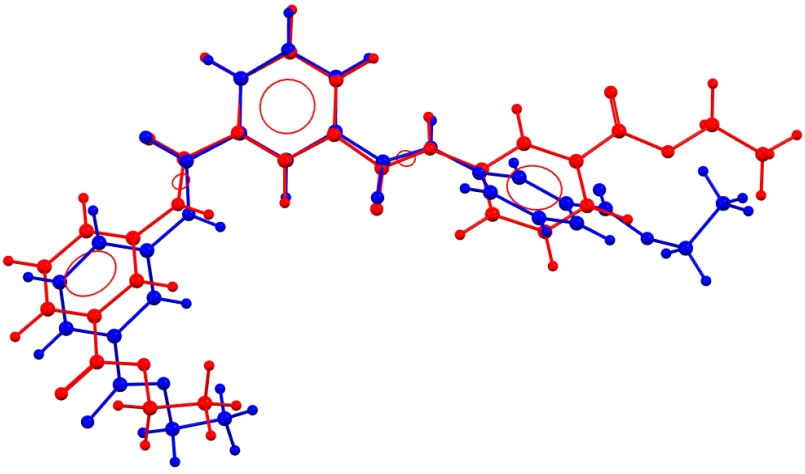

(**D3E**) (**A**)

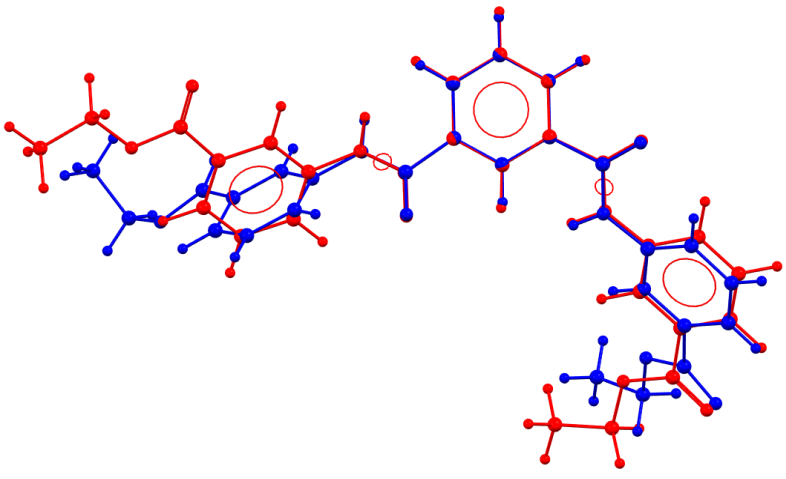

D3E (**molecule B**)

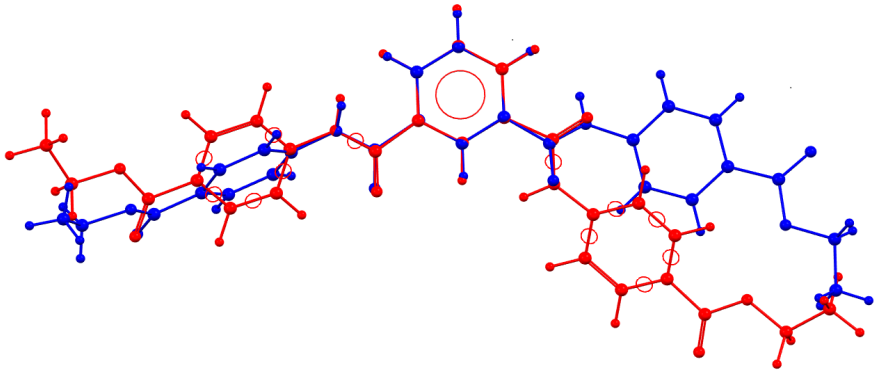

(**D4E**)

S9. DxE Molecular Overlay

The molecular overlap is reasonable for **D3E**, but there are more groups and atoms that differ between the **optimised structures** and **crystal structures** in the **D2E** and **D4E** molecules. In **D2E**, the calculated structure adopts the ***syn–syn*** conformation, whereas in the **D2E** crystal structure, the molecular conformation has the ***anti–anti*** conformation, as stabilised by intramolecular interactions.

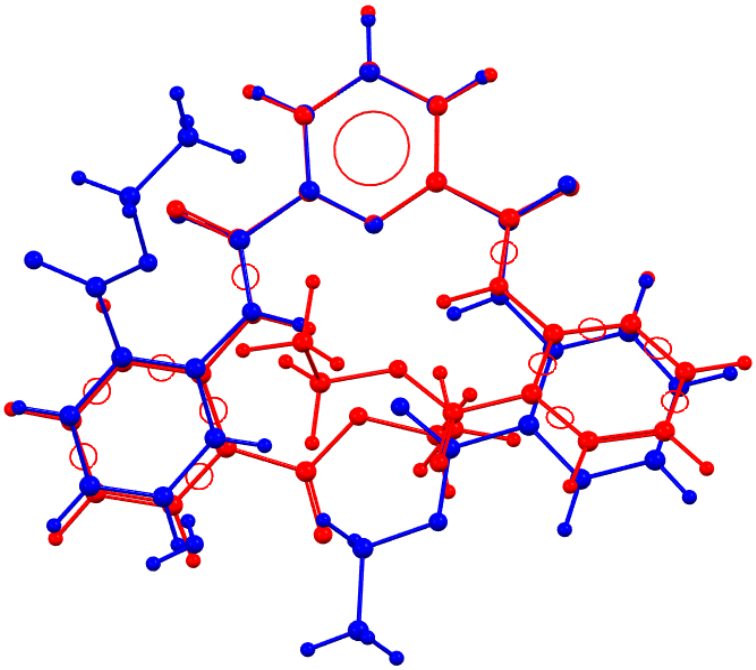

(**P2E**)

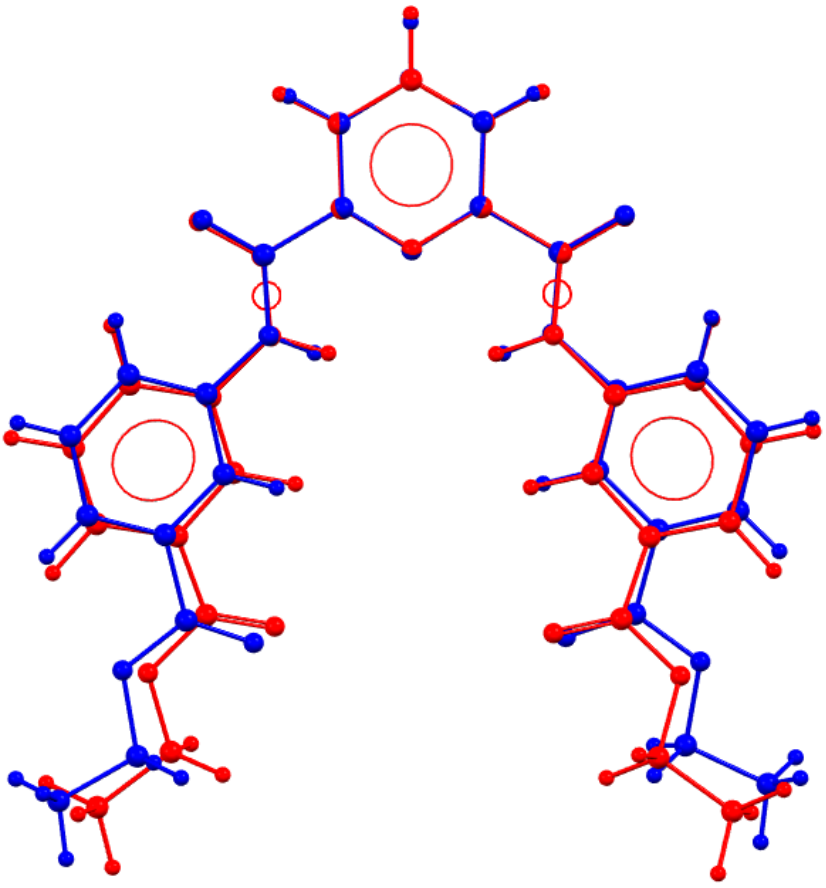

(**P3E**)

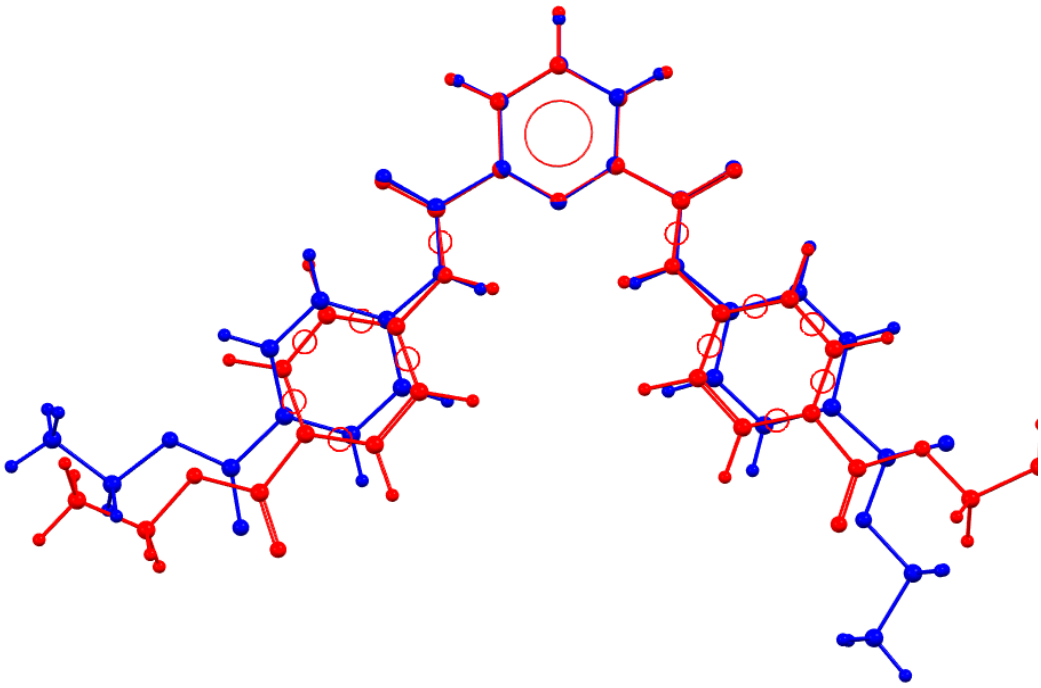

(**P4E**)

S10. PxE Molecular Overlay

The overlay of the three **PxE** molecules (**optimised** and **molecular structures**) is at an optimum for **P3E** and **P4E**, with only some small deviations in one of the ester group orientations in **P4E**. For **P2E**, the differences are considerably greater, but the overlap is good for the central three aromatic rings, and with the orientation of the benzene ester flipped by 180° for one of the rings. The water molecules (in **PxE**) are not included in the molecular overlay calculations and diagrams.

Table S3. Statistical analysis of intermolecular contacts on the Hirshfeld surface. The chemical content on the Hirshfeld surface, the % of contact types (C_{XY}) and their enrichment ratios are shown. The major surface components, major C_{XY} contacts and significantly enriched contacts ($E > 1$) are highlighted in **bold**. Enrichment ratios related to very small parts of the Hirshfeld surface (N and H_{ON}) are omitted, as they are not pertinent [30].

Surface (%)	**D2E**	**D3E**	**D4E**	**P2E_W**	**P2E_W2**	**P4E_W2**
H_{ON}	1.0	2.6	3.1	6.4	11.8	12.4
C	**39.6**	**30.3**	**33.7**	**31.4**	**28.8**	**28.3**
N	1.6	1.2	1.3	2.5	2.5	2.3
O	10.9	8.4	12.8	14.8	15.8	16.0
H_C	**47.0**	**45.1**	**49.1**	**45.0**	**41.2**	**41.0**
Contacts (%)	**D2E**	**D3E**	**D4E**	**P2E_W**	**P3E_W2**	**P4E_W2**
$H_{ON}\cdots H_{ON}$	0.0	0.0	0.0	0.0	0.3	1.6
$C\cdots H_{ON}$	2.0	1.8	1.1	7.2	4.0	1.5
$N\cdots H_{ON}$	0.0	0.0	0.0	0.0	0.1	0.0
$O\cdots H_{ON}$	0.0	3.8	4.3	2.2	11.5	12.4
$H_C\cdots H_{ON}$	0.0	0.0	0.9	4.2	8.4	8.8
C···C	**21.3**	**15.6**	8.9	**11.4**	**11.8**	**15.1**
N···C	3.2	2.4	0.6	3.4	1.7	3.0
O···C	7.9	5.7	4.6	5.3	6.3	4.7
$H_C\cdots C$	**22.2**	**28.2**	**42.7**	**21.9**	**21.4**	**17.4**
N···N	0.0	0.0	0.0	0.1	0.3	0.1
O···N	0.0	0.1	0.0	0.2	0.4	0.1
$H_C\cdots N$	0.0	0.1	2.1	1.2	2.2	1.3
O···O	0.3	0.4	0.8	0.2	0.0	0.4
$H_C\cdots O$	**12.7**	**14.8**	**15.6**	**21.5**	**14.0**	**14.2**
$H_C\cdots H_C$	**30.6**	**27.1**	**18.3**	**21.5**	**17.8**	**19.7**
Enrichment	**D2E**	**D3E**	**D4E**	**P2E_W**	**P3E_W2**	**P4E_W2**
$H_{ON}\cdots H_{ON}$	/	/	/	0.00	0.22	0.95
$C\cdots H_{ON}$	2.57	0.93	0.52	1.75	0.57	0.20
$N\cdots H_{ON}$	/	/	/	0.11	0.15	0.00
$O\cdots H_{ON}$	0.00	**5.24**	**5.21**	1.09	**2.90**	**2.99**
$H_C\cdots H_{ON}$	0.00	0.02	0.30	0.67	0.84	0.84
C···C	**1.41**	**1.31**	0.80	**1.25**	**1.45**	**1.87**
N···C	2.57	2.74	0.67	2.26	1.21	2.32
O···C	0.96	0.65	0.52	0.59	0.69	0.51
$H_C\cdots C$	0.59	0.84	**1.30**	0.79	0.93	0.76
N···N	/	/	/	/	/	/
O···N	0.00	0.20	0.00	0.26	0.55	0.08
$H_C\cdots N$	0.00	0.06	1.58	0.52	1.08	0.67
O···O	0.24	0.27	0.46	0.07	0.01	0.14
$H_C\cdots O$	1.25	1.18	1.22	1.59	1.07	1.09
$H_C\cdots H_C$	1.33	1.16	0.76	1.02	1.07	1.20

S11. Fingerprint (FP) Plots for D2E–P4E

The two-dimensional fingerprint (FP) plots used for visualising and quantifying intermolecular interactions were obtained with CrystalExplorer17 software [28] and are available in the **ESI** (pp. 43–49). All of the FP plots show two spikes at short distances corresponding to the strong O-H···O and O-H···N hydrogen bonds. These spikes are observed at larger distances in the compound **D2E**, as they correspond to weaker C-H···O interactions, as the intramolecular strong H-bond is not accounted for. All six compounds show similar patterns for H···H and C···H interactions, which appear quite abundant.

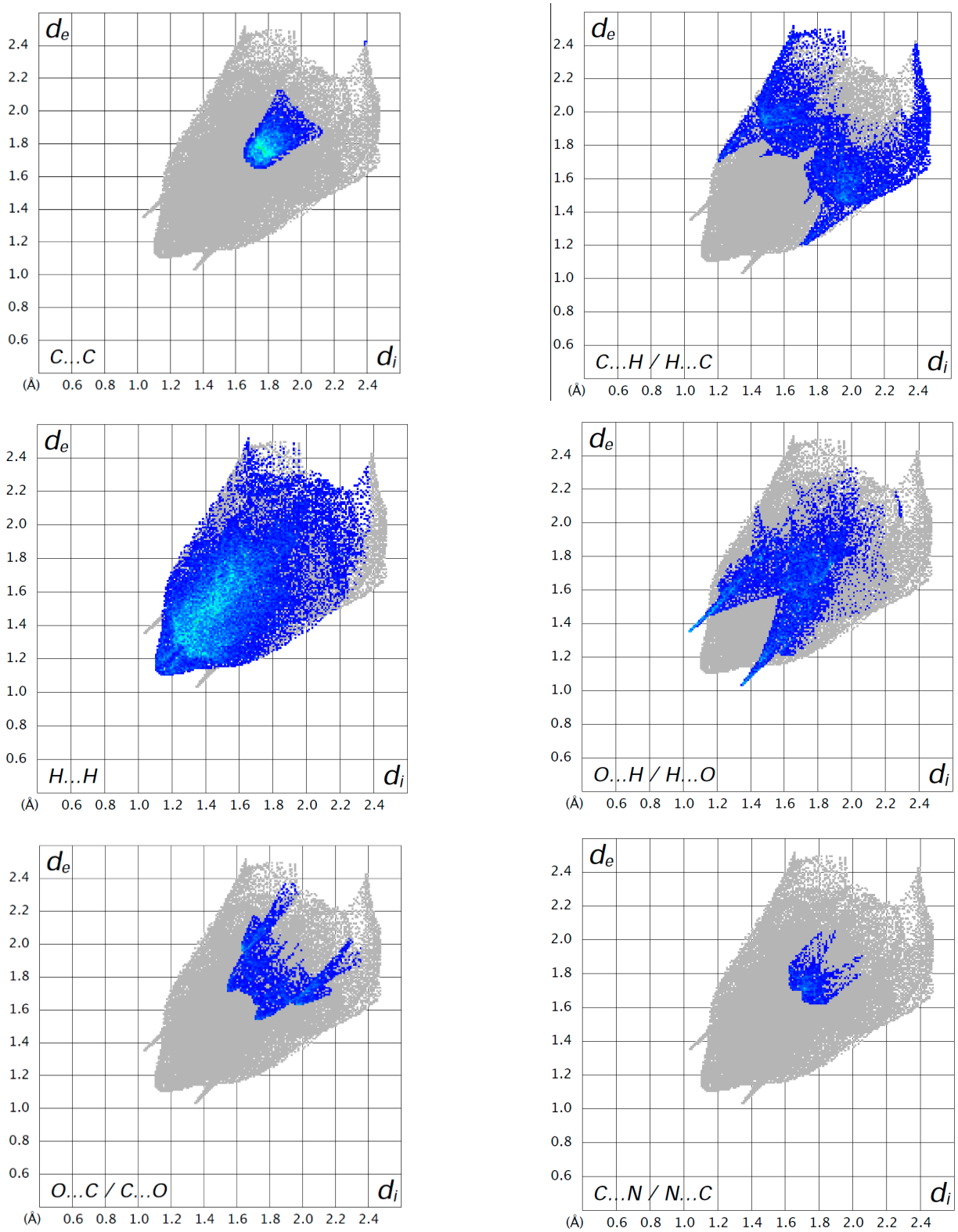

Figure Sup_FP_D2E. Fingerprint plots of the main interactions on the Hirshfeld surface for **D2E**.

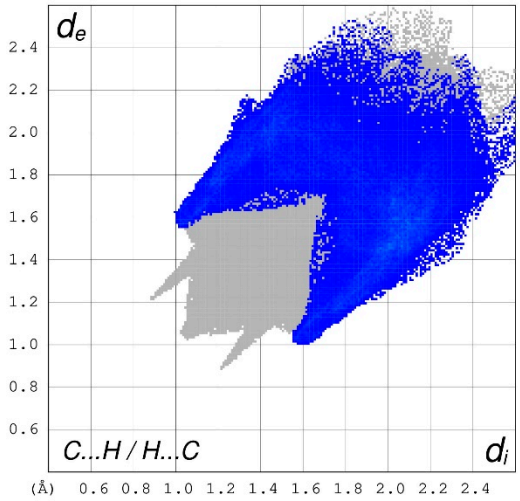
d_e
2.4
2.2
2.0
1.8
1.6
1.4
1.2
1.0
0.8
0.6
C...H / H...C
d_i
(Å) 0.6 0.8 1.0 1.2 1.4 1.6 1.8 2.0 2.2 2.4

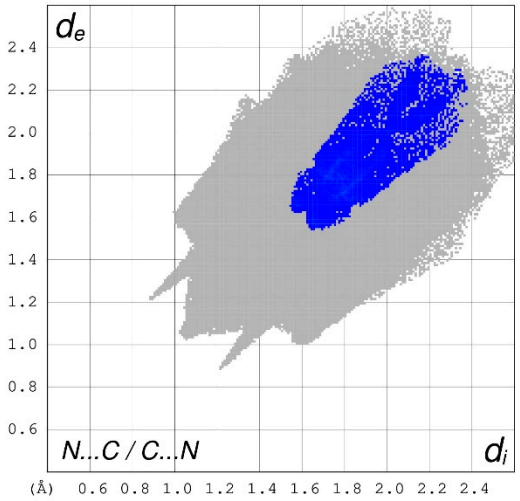
d_e
2.4
2.2
2.0
1.8
1.6
1.4
1.2
1.0
0.8
0.6
N...C / C...N
d_i
(Å) 0.6 0.8 1.0 1.2 1.4 1.6 1.8 2.0 2.2 2.4

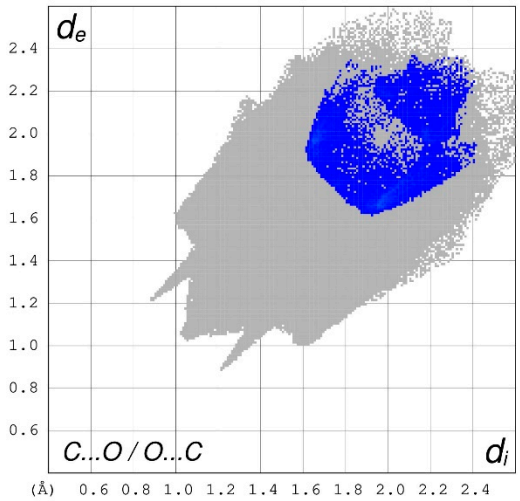
d_e
2.4
2.2
2.0
1.8
1.6
1.4
1.2
1.0
0.8
0.6
C...O / O...C
d_i
(Å) 0.6 0.8 1.0 1.2 1.4 1.6 1.8 2.0 2.2 2.4

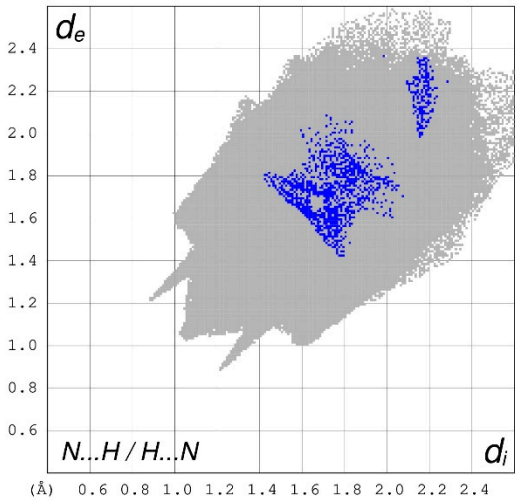
d_e
2.4
2.2
2.0
1.8
1.6
1.4
1.2
1.0
0.8
0.6
N...H / H...N
d_i
(Å) 0.6 0.8 1.0 1.2 1.4 1.6 1.8 2.0 2.2 2.4

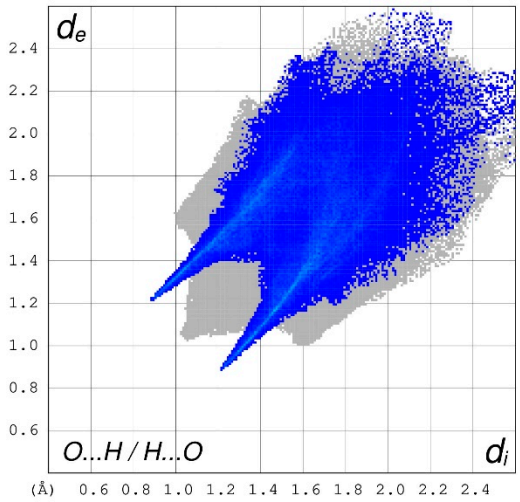
d_e
2.4
2.2
2.0
1.8
1.6
1.4
1.2
1.0
0.8
0.6
O...H / H...O
d_i
(Å) 0.6 0.8 1.0 1.2 1.4 1.6 1.8 2.0 2.2 2.4

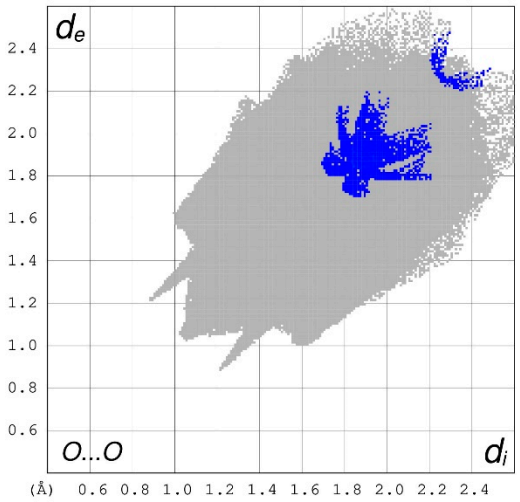
d_e
2.4
2.2
2.0
1.8
1.6
1.4
1.2
1.0
0.8
0.6
O...O
d_i
(Å) 0.6 0.8 1.0 1.2 1.4 1.6 1.8 2.0 2.2 2.4

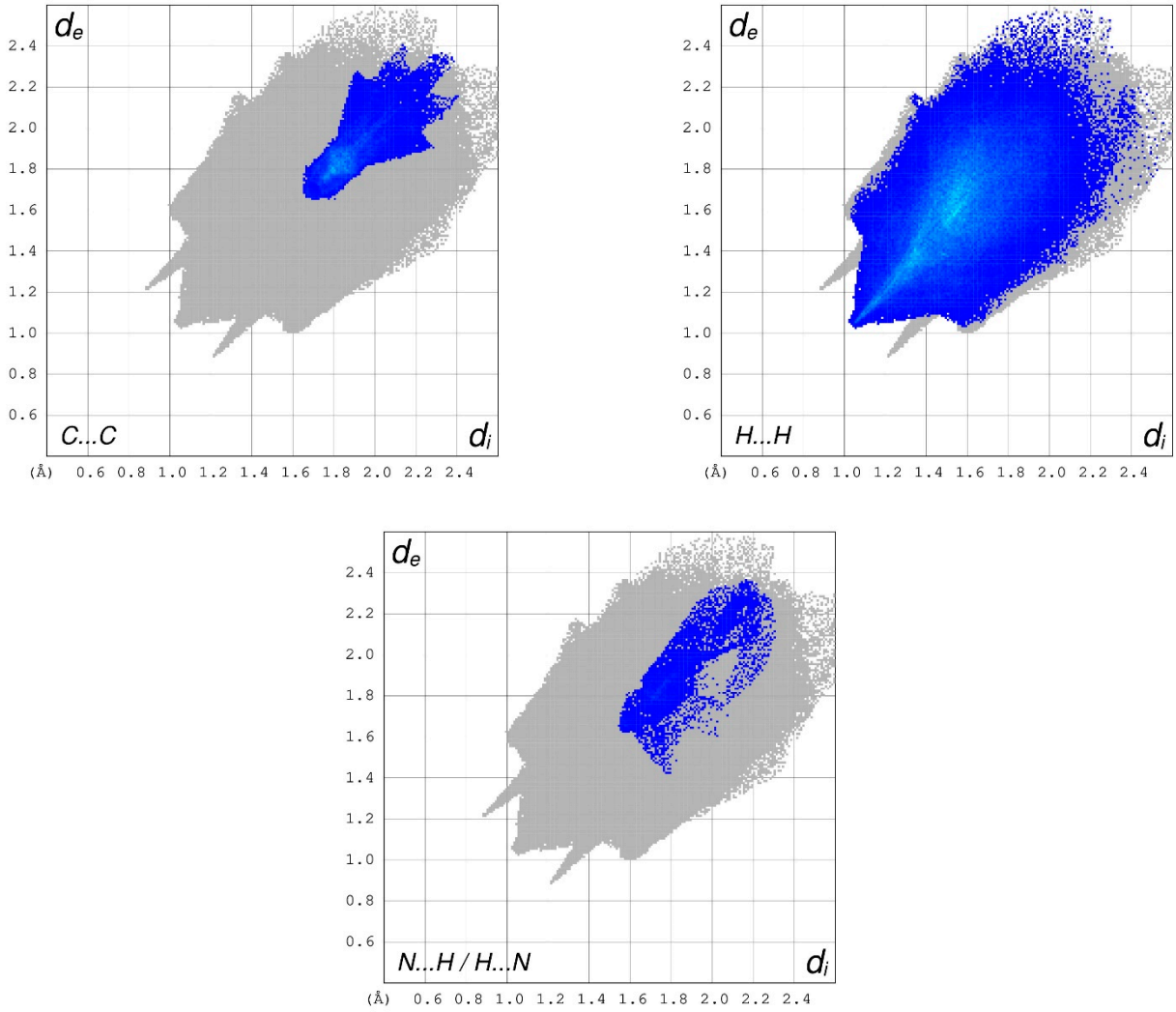

Figure Sup_FP_D3E. Fingerprint plots of the main interactions on the Hirshfeld surface for **D3E**.

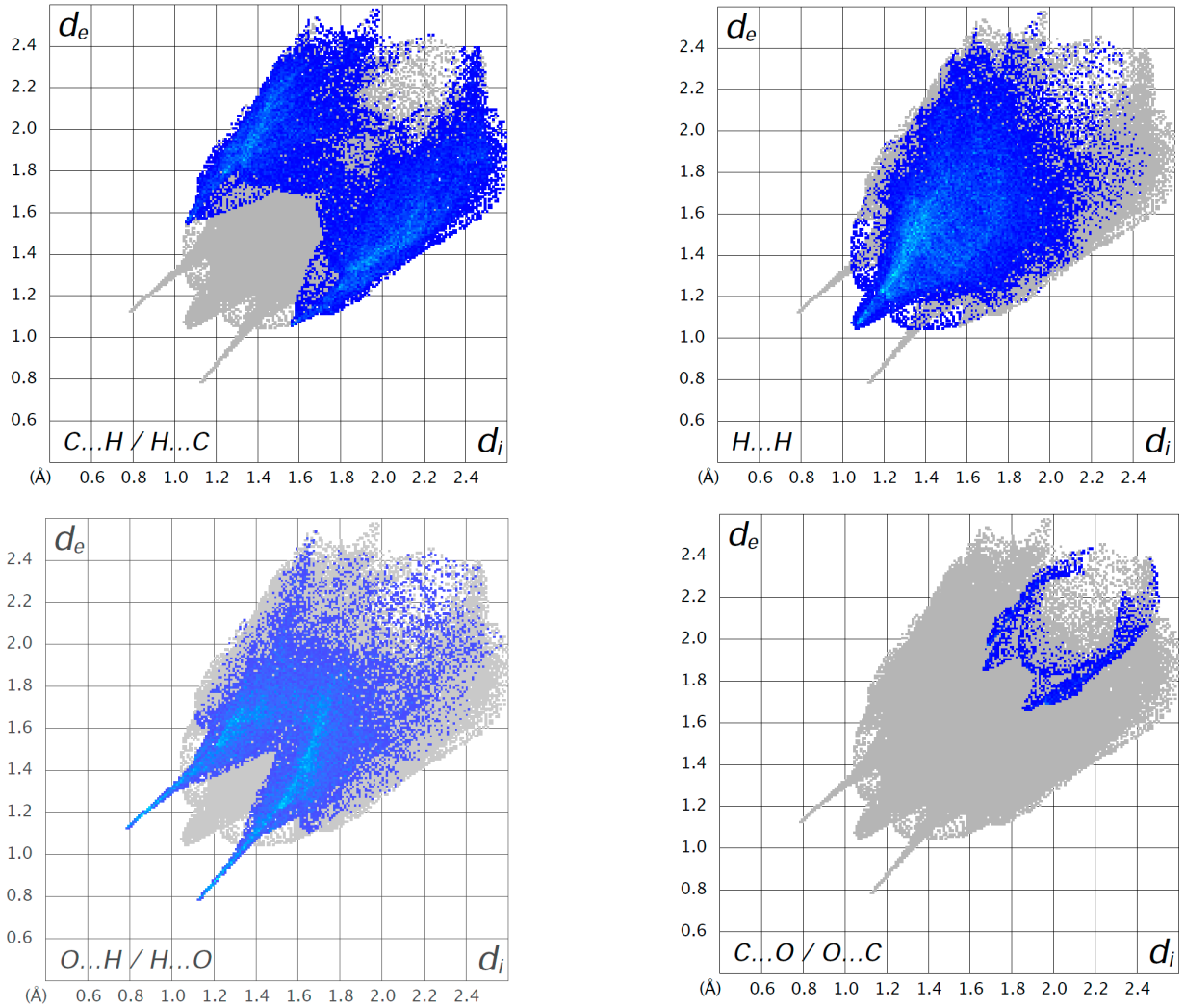

Figure Sup_FP_D4E. Fingerprint plots of the main interactions on the Hirshfeld surface for **D4E**.

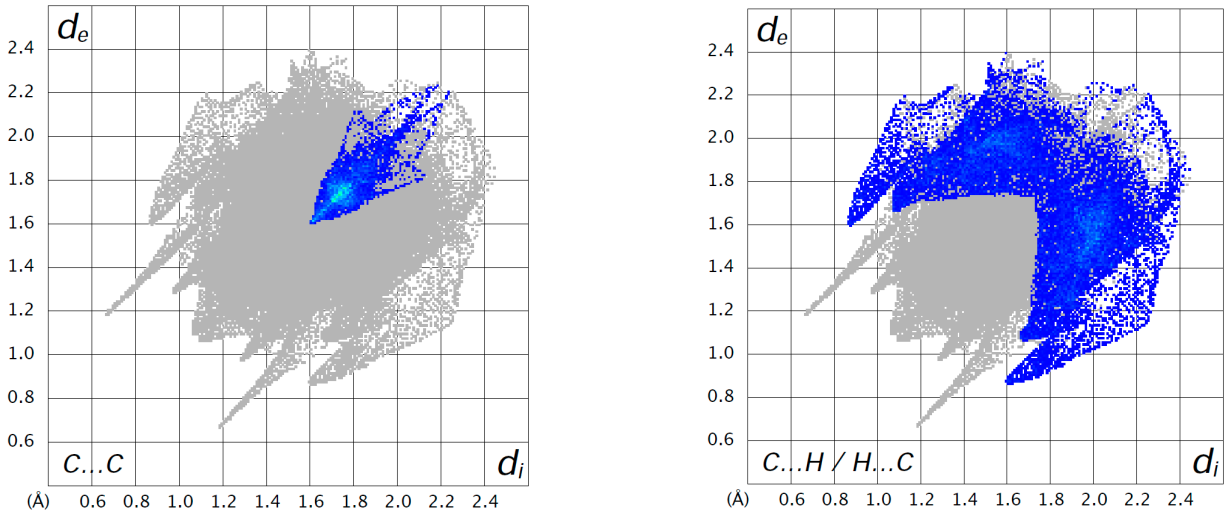

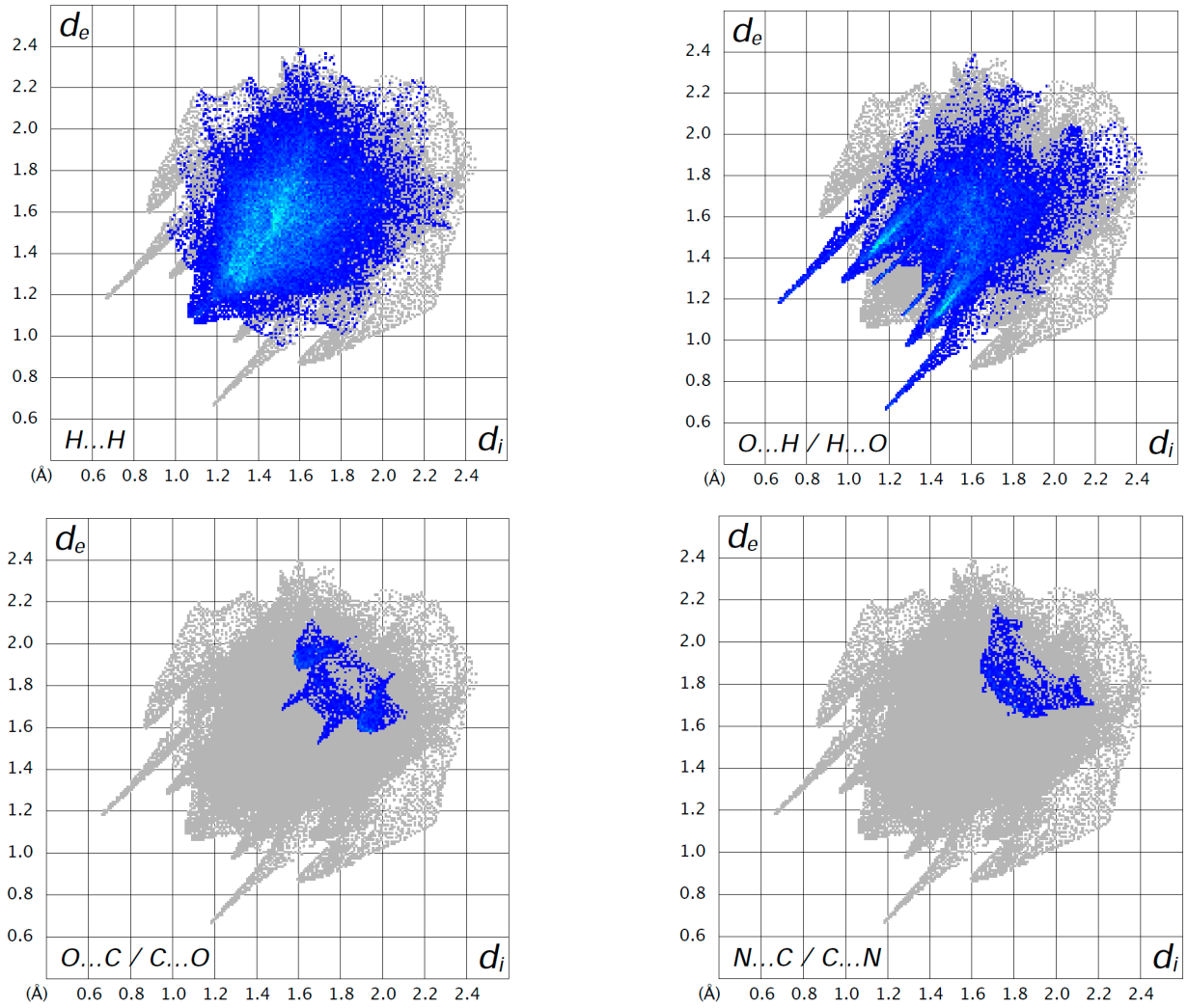

Figure Sup_FP_P2E. Fingerprint plots of the main interactions on the Hirshfeld surface for **P2E_W**.

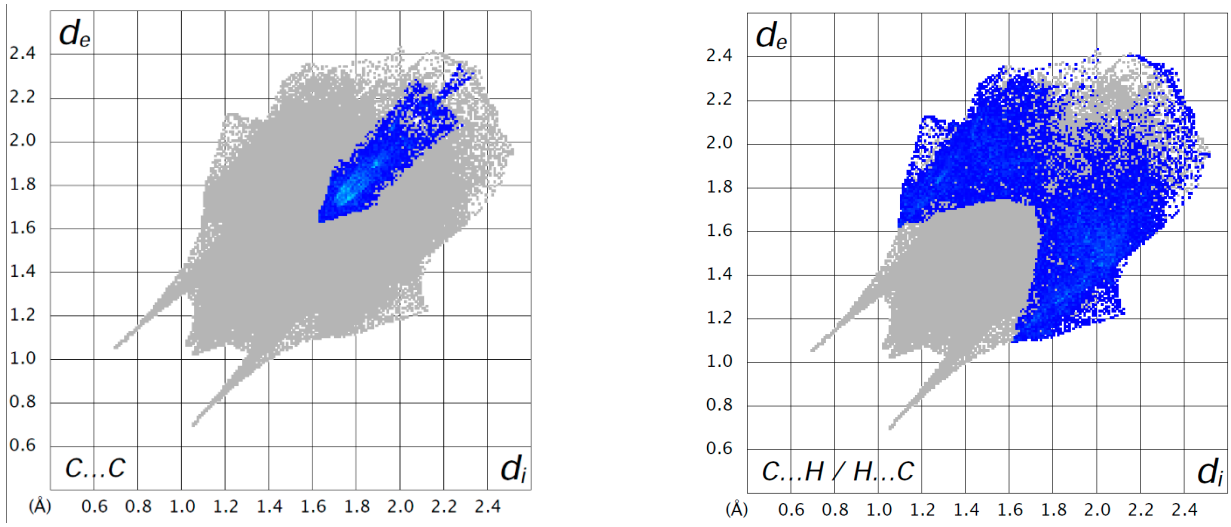

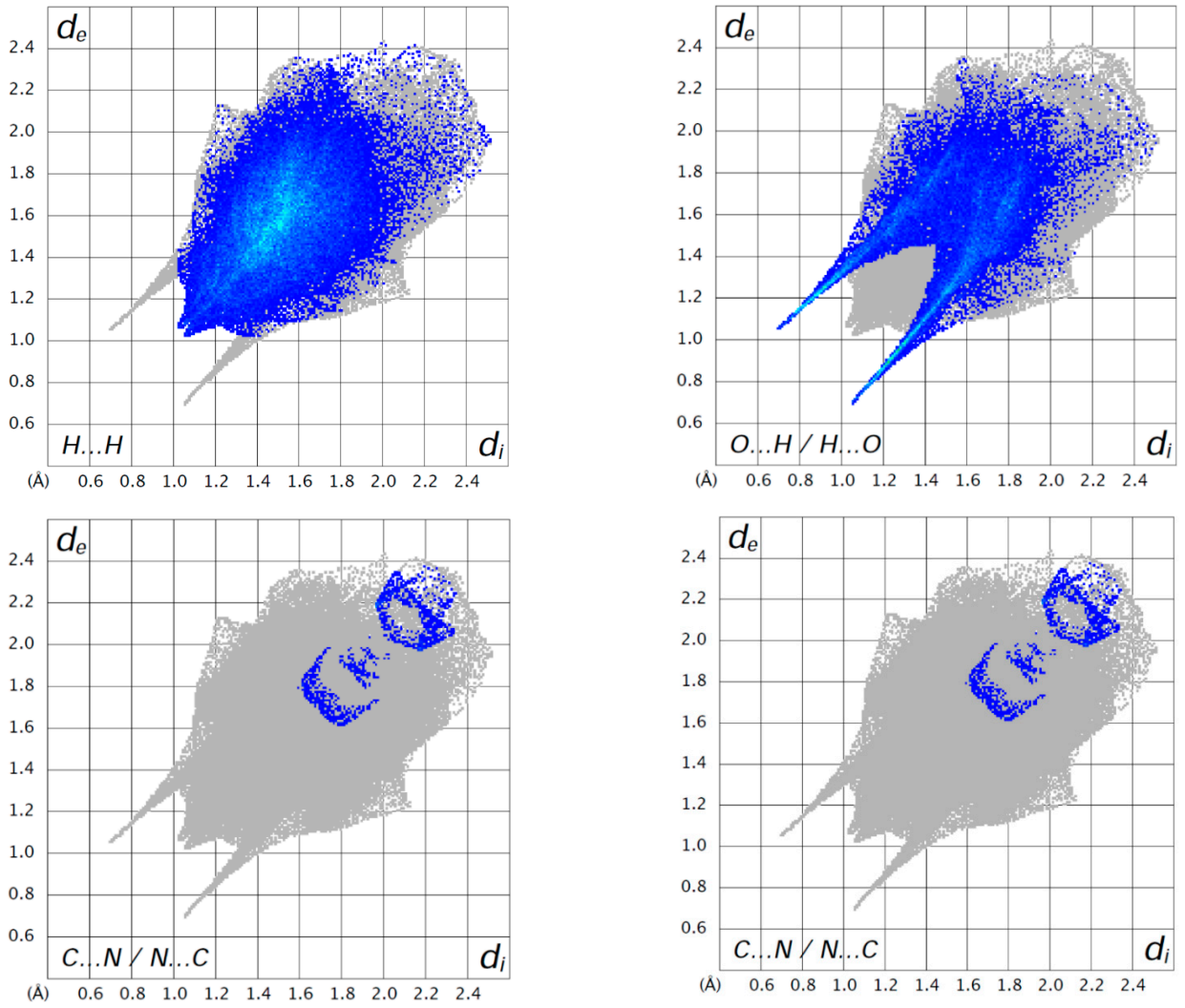

Figure Sup_FP_P3E. Fingerprint plots of the main interactions on the Hirshfeld surface for **P3E**.

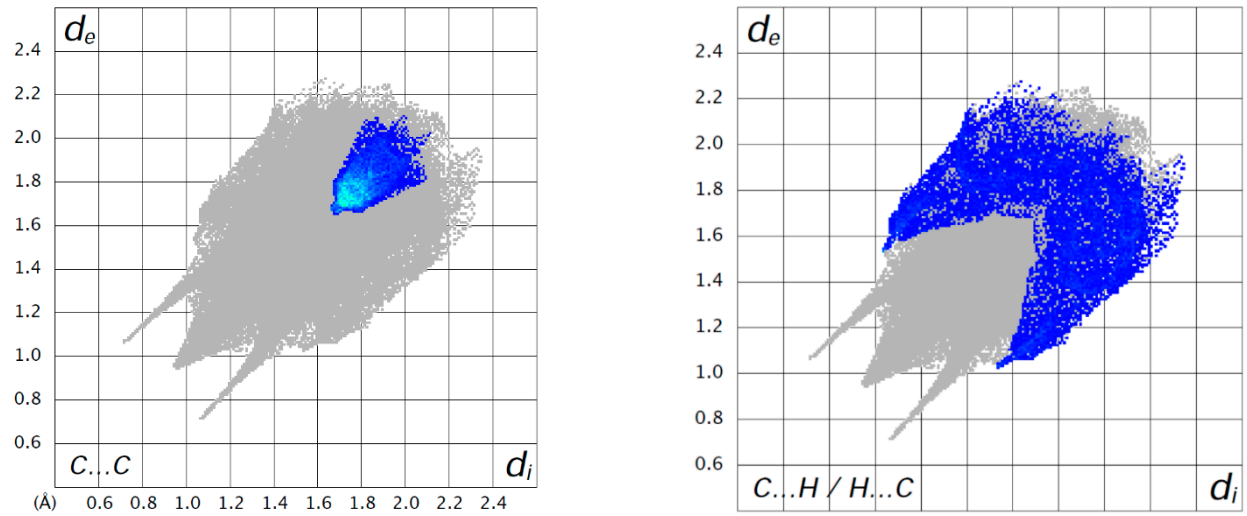

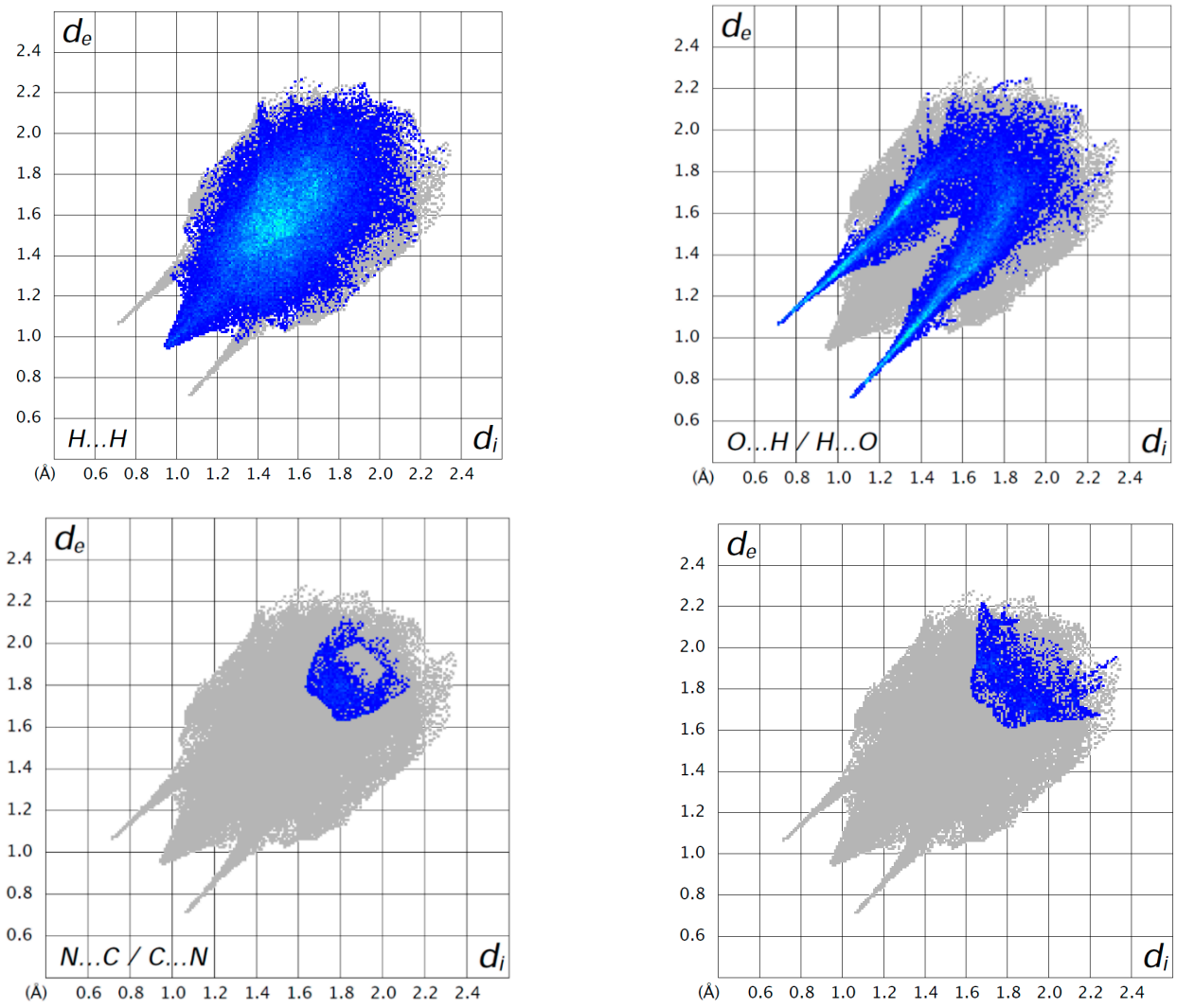

Figure Sup_FP_P4E. Fingerprint plots of the main interactions on the Hirshfeld surface for **P4E**.